Bulletin of Mathematical Biology (2024) 86:67
https://doi.org/10.1007/s11538-024-01296-y

Society for Mathematical Biology

ORIGINAL ARTICLE

Evolution of Cooperation in Spatio-Temporal Evolutionary Games with Public Goods Feedback

Haihui Cheng[1,2] · Liubov Sysoeva[2] · Hao Wang[2] · Hairui Yuan[1] · Tonghua Zhang[3] · Xinzhu Meng[1]

Received: 24 January 2024 / Accepted: 8 April 2024

Abstract

In biology, evolutionary game-theoretical models often arise in which players' strategies impact the state of the environment, driving feedback between strategy and the surroundings. In this case, cooperative interactions can be applied to studying ecological systems, animal or microorganism populations, and cells producing or actively extracting a growth resource from their environment. We consider the framework of eco-evolutionary game theory with replicator dynamics and growth-limiting public goods extracted by population members from some external source. It is known that the two sub-populations of cooperators and defectors can develop spatio-temporal patterns that enable long-term coexistence in the shared environment. To investigate this phenomenon and unveil the mechanisms that sustain cooperation, we analyze two eco-evolutionary models: a well-mixed environment and a heterogeneous model with spatial diffusion. In the latter, we integrate spatial diffusion into replicator dynamics. Our findings reveal rich strategy dynamics, including bistability and bifurcations, in the temporal system and spatial stability, as well as Turing instability, Turing–Hopf bifurcations, and chaos in the diffusion system. The results indicate that effective mechanisms to promote cooperation include increasing the player density, decreasing the relative timescale, controlling the density of initial cooperators, improving the diffusion rate of the public goods, lowering the diffusion rate of the cooperators, and enhancing the payoffs to the cooperators. We provide the conditions for the existence, stability, and occurrence of bifurcations in both systems. Our analysis can be applied to dynamic phenomena in fields as diverse as human decision-making, microorganism growth factors secretion, and group hunting.

✉ Xinzhu Meng
mxz721106@sdust.edu.cn

[1] College of Mathematics and Systems Science, Shandong University of Science and Technology, Qingdao 266590, People's Republic of China

[2] Department of Mathematical and Statistical Sciences, University of Alberta, Edmonton, AB T6G 2G1, Canada

[3] Department of Mathematics, Swinburne University of Technology, Hawthorn, VIC 3122, Australia

Published online: 03 May 2024

Keywords Evolutionary game theory · Replicator dynamics · Pattern formation · Spatial dynamics · Turing–Hopf bifurcation · Chaotic pattern

1 Introduction

Social dilemmas arise from conflicts between individual and collective interests and are observed in various domains, including humans (Bonnefon et al. 2016; Kummerli et al. 2007; Li et al. 2018; Heggerud et al. 2022), animals (Cheng et al. 2022; Riehl and Frederickson 2016; Yamaguchi and Iwasa 2021), and microorganisms (Wakano et al. 2009; Behar et al. 2014; Lynn and De Leenheer 2019). Sustainable development necessitates individual contributions and sacrifices for the collective good, such as air, water, fossil fuels, and fisheries. In animal groups, food obtained through group hunting efforts may be shared with non-contributing individuals (Cheng et al. 2022; Lett et al. 2004). Microorganisms secrete beneficial growth factors at a cost to acquire nutrients, allowing others to exploit their efforts (Schuster et al. 2010; Smith and Schuster 2019). Defectors exploit public resources without cost, potentially leading to a tragedy of the commons (Milinski et al. 2002; Rankin et al. 2007). Despite the risks associated with selfish behavior, cooperative behavior is prevalent in nature and human society, making it crucial to comprehend the underlying mechanisms sustaining cooperation. Evolutionary game theory (Hofbauer and Sigmund 1998) is a vital framework for studying cooperation, with replicator dynamics (Nowak 2006) being widely employed.

Cooperation in populations is triggered by the production of public goods, which are essential for individual growth and development. Cooperators incur costs in order to produce or capture these shared resources, benefiting the entire population. The presence of public goods fosters an environment conducive to cooperation. The cooperative or non-cooperative behaviors of individuals have an impact on the availability of public goods, which then affects players' strategy choices. The term 'eco-evolutionary games' corresponds to scenarios where evolutionary game dynamics are environmentally coupled. This mutual feedback between public goods dynamics and strategy dynamics (Weitz et al. 2016; Hauert et al. 2019; Tilman et al. 2020; Cheng et al. 2023) was often overlooked in previous studies, which predominantly focused on economic aspects and neglected the interplay between public goods and strategies within the replicator dynamics framework (Charness et al. 2014; Lotito et al. 2013; Fallucchi et al. 2019). To address this gap, we combine replicator dynamics with public goods dynamics to construct an evolutionary game system with public goods feedback, enabling an exploration of the impact of public goods feedback on the evolution of cooperation.

Spatial diffusion plays a crucial role in strategy evolution. Based on Fick's law, matter in space exhibits heterogeneous distribution due to diffusion, which has been experimentally confirmed in microorganisms such as *Escherichia coli* (Kerr et al. 2002; Kirkup and Riley 2004; Conlin et al. 2014; Lambert et al. 2014), yeasts (MacLean and Gudelj 2006; Schuster et al. 2010), *Pseudomonas aeruginosa* (Wang et al. 2015; Griffin et al. 2004; Figueiredo et al. 2021; Mridha and Kummerli 2022), and *Bacillus subtilis* (Ratzke and Gore 2016). Cressman and Vickers (1997) examined density-dependent game models in one spatial dimension and demonstrated resistance to strategy invasion. Hauert (2002) compared spatially expanding populations to well-

mixed populations and observed that spatial expansion promotes cooperation in 2×2 games. Aydogmus (2018) incorporated spatial effects into the classical hawk-dove game and revealed the disruption of evolutionarily stable strategies at low diffusion rates. However, the pattern formation of strategies in replicator dynamics with spatial diffusion remains unclear. Introducing spatial diffusion into replicator dynamics is challenging due to the emphasis on frequency rather than density variation. In this study, we convert player frequencies to player densities, allowing for the incorporation of spatial diffusion into replicator dynamics. Thus, we enable analysis of the spatio-temporal pattern formation in the framework of the eco-evolutionary model with both spatial diffusion and improved replicator dynamics.

While complex patterns are prevalent in physics and chemistry (Maini et al. 1997; Walgraef 2012; Deegan 2000), they also manifest in biological systems (Song et al. 2022, 2021; Manna et al. 2021). Previous studies have extensively explored spatial patterns in prey-predator systems (Chowdhury et al. 2021a; Pal et al. 2020, 2021; Jia et al. 2019; Yan et al. 2020) and infectious disease systems (Li et al. 2014; Berres and Ruiz-Baier 2011; Sun et al. 2009). Nevertheless, the spatial dynamics and patterns of cooperation in evolutionary game systems with public goods feedback remain understudied. In this analysis, we introduce spatial diffusion into the system by combining improved replicator dynamics with public goods dynamics. Our objective is to investigate the spatial strategy dynamics and patterns of cooperation in this eco-evolutionary game system.

The structure of this paper is as follows. In Sect. 2, we construct temporal and diffusion systems. In Sect. 3, we examine the existence and bistability of equilibria, provide conditions for transcritical and Hopf bifurcations, as well as investigate the direction and stability of the periodic solution. In Sect. 4, we analyze the local stability, Turing instability, and Turing–Hopf bifurcation of the diffusion system. In Sect. 5, we explore the effects of parameters and diffusion coefficients on the spatial distribution of cooperation, leading to diverse spatial patterns. We summarize and discuss our findings in Sect. 6.

2 Model Formulation

2.1 Temporal System

Consider a situation where individuals acquire resources from their surroundings to benefit an entire population, such as predators hunting in groups or cells extracting iron from some external substrate. Examine a scenario where every individual in a population can fall into one of two categories: cooperators or defectors. Cooperators put in some effort to produce public goods, while defectors directly cheat the cooperators to acquire resources. In our model, cooperative interaction only affects the enrichment process of public goods. Both cooperators and defectors consume resources to maintain their vital activities. Suppose that the growth-limiting public goods are extracted from some external source. Thus, the rate of public goods production should be bounded even for high densities of productive population. According to Behar et al. (2014), in this case, the production of public goods can be written in the form of $\frac{\beta u}{\alpha+u}$.

Assuming a linear consumption rate of the public goods, the dynamics of the resource can be represented by the following equation:

$$\frac{dm}{dT} = \frac{\beta u}{\alpha + u} - kNm, \tag{2.1}$$

where β, α, and k are the maximum productivity, the saturation parameter of production, and the consumption rate for public goods, respectively; $u \in [0, N]$ and N depict the density of cooperators and that of all players, respectively; m is the concentration of public goods. Constants β, α, k, and N are positive. The density of defectors can be denoted as $v = N - u$. Converting the densities of cooperators and defectors into frequencies gives $\xi_1 = \frac{u}{N}$ and $\xi_2 = \frac{v}{N} = 1 - \frac{u}{N}$.

The payoffs in the game are influenced not only by the cooperation (C) and defection (D) strategies players adopt, but also by the concentration of public goods. Hence, we assume payoffs in the game to be a weighted linear combination of payoff matrices under poor and rich public goods conditions, where weights depend on resource concentration. Thus, the payoff matrix can be written as

$$\Pi = (\delta - m) \begin{matrix} \\ C \\ D \end{matrix} \begin{matrix} \begin{matrix} C & \quad D \end{matrix} \\ \begin{pmatrix} A_0 - \sigma_0 & B_0 - \sigma_0 \\ c_0 & d_0 \end{pmatrix} \end{matrix} + m \begin{matrix} \\ C \\ D \end{matrix} \begin{matrix} \begin{matrix} C & \quad D \end{matrix} \\ \begin{pmatrix} A_1 - \sigma_1 & B_1 - \sigma_1 \\ c_1 & d_1 \end{pmatrix} \end{matrix},$$

where $\delta > 0$ represents baseline payoffs when $m = 0$. In the literature (Weitz et al. 2016; Tilman et al. 2020), it is usually assumed that $\delta = 1$. In our study, we expand δ to be any positive value, since the concentration of public goods is not restricted to the interval [0, 1]. This enables us to study better the impact of δ on the game dynamics. The cost of cooperation varies in different environments, while defectors do not bear the cost of cooperation (Hauert et al. 2019). Parameters $\sigma_0 > 0$ and $\sigma_1 > 0$ represent the costs of producing public goods under different environmental conditions. Later, we will study the effect of payoffs on the concentration of public goods and the density of cooperators. To enable independent consideration of each payoff, we rewrite the payoff matrix as

$$\Pi = (\delta - m) \begin{matrix} \\ C \\ D \end{matrix} \begin{matrix} \begin{matrix} C & \quad D \end{matrix} \\ \begin{pmatrix} a_0 & b_0 \\ c_0 & d_0 \end{pmatrix} \end{matrix} + m \begin{matrix} \\ C \\ D \end{matrix} \begin{matrix} \begin{matrix} C & \quad D \end{matrix} \\ \begin{pmatrix} a_1 & b_1 \\ c_1 & d_1 \end{pmatrix} \end{matrix},$$

where $a_0 = A_0 - \sigma_0$, $b_0 = B_0 - \sigma_0$, $a_1 = A_1 - \sigma_1$, and $b_1 = B_1 - \sigma_1$. Now we calculate the fitness of strategies C and D:

$$\begin{aligned} f_C(u, m) &= (\delta a_0 + (a_1 - a_0)m)\frac{u}{N} + (\delta b_0 + (b_1 - b_0)m)\left(1 - \frac{u}{N}\right), \\ f_D(u, m) &= (\delta c_0 + (c_1 - c_0)m)\frac{u}{N} + (\delta d_0 + (d_1 - d_0)m)\left(1 - \frac{u}{N}\right). \end{aligned} \tag{2.2}$$

The incentives of behavioral changes can be explained by the following combinations of elements in the payoff matrix.

$$\begin{aligned}
\Gamma_1 &= f_C(0,\delta) - f_D(0,\delta) = \delta(b_1 - d_1),\\
\Gamma_2 &= f_C(N,\delta) - f_D(N,\delta) = \delta(a_1 - c_1),\\
\Phi_1 &= f_D(N,0) - f_C(N,0) = \delta(a_0 - c_0),\\
\Phi_2 &= f_D(0,0) - f_D(0,0) = \delta(d_0 - b_0).
\end{aligned}$$

Parameter Γ_1 depicts the incentive for an individual within the population to choose cooperation when other players in the population are defectors, and the public goods are abundant. Parameter Γ_2 depicts the incentive for an individual to follow suit and become a cooperator when other players are already cooperators in a setting where the public goods are affluent. Parameter Φ_1 depicts the incentive for an individual to turn defector in a state where the public goods are scarce and other individuals in the population are cooperators. Finally, parameter Φ_2 depicts the incentive for an individual to follow a shift to strategy D when other players in the population have adopted strategy D and the public goods are barren. These parameters obtained from the payoff matrix explain the motivations that drive players to change their strategies. Thus, the payoff matrix can be determined arbitrarily regardless of cooperative interaction.

The replicator dynamics (Hofbauer and Sigmund 1998) is a model used to describe the evolution of populations. It assumes that the frequency of a strategy increases when the fitness of those who adopt it is greater than the average fitness of the population. Replicator dynamics has previously been used to model behavioural changes in settings at the interface of ecology and game theory, such as economic activity around a coral reef being based on fishing or tourism (Milne et al. 2022) and eutrophication in shallow lakes where the discharge of pollutants into the water is determined by a behavioural model (Sun and Hilker 2021). Coupling Eq. (2.1) with replicator dynamics, and accounting for potentially different rates of environmental and strategic change, we obtain the public goods game system as follows:

$$\begin{cases}
\varepsilon \frac{\mathrm{d}u}{\mathrm{d}T} = u\left(1 - \frac{u}{N}\right)(f_C - f_D),\\
\frac{\mathrm{d}m}{\mathrm{d}T} = \frac{\beta u}{\alpha + u} - kNm,
\end{cases}$$

in which $\varepsilon > 0$ is the relative timescale for evolutionary rate of public goods compared to that of strategies. The inequality $\varepsilon > 1$ ($\varepsilon < 1$) means that public goods evolve faster (slower) than strategies. Rescaling the time by substitution $t = \frac{T}{\varepsilon}$ and using equalities (2.2), we rewrite the system as

$$\begin{cases}
\dfrac{\mathrm{d}u}{\mathrm{d}t} = \dfrac{u}{N^2}(N-u)\left[(\eta_1 u + N\eta_2)m - \delta(\eta_3 u + N(d_0 - b_0))\right],\\
\dfrac{\mathrm{d}m}{\mathrm{d}t} = \varepsilon\left(\dfrac{\beta u}{\alpha + u} - kNm\right),
\end{cases} \tag{2.3}$$

where

$$\eta_1 = a_1 - a_0 + b_0 - b_1 + c_0 - c_1 + d_1 - d_0, \quad \eta_2 = d_0 - d_1 + b_1 - b_0,$$
$$\eta_3 = b_0 + c_0 - a_0 - d_0.$$

Thus, we have developed a game system that depicts cooperative behavior with mutual feedback between strategy and surroundings within a well-mixed environment. This model is well-suited for describing planktonic cultures, where molecules diffuse rapidly and all bacteria experience the same concentration (Julou et al. 2013).

2.2 Diffusion System

The spatial distribution of cooperators and the public goods they produce can significantly affect the process of evolution. The evolution of cooperation exhibits significant differences under homogeneous and heterogeneous conditions, ranging from the extinction of cooperators to the coexistence of both cooperators and defectors (Julou et al. 2013; MacLean and Gudelj 2006). There is a range of experiments done to investigate the cooperation of yeast (MacLean and Gudelj 2006), *Escherichia coli* (Lambert et al. 2014; Kirkup and Riley 2004), and *Pseudomonas aeruginosa* (Julou et al. 2013) within heterogeneous environments. Thus, to account for the dynamic spatial nature of strategies and public goods, we introduce diffusion into the temporal system (2.3) as follows:

$$\begin{cases} \frac{\partial u(\mathbf{x},t)}{\partial t} = \frac{u}{N^2}(N-u)[(\eta_1 u + N\eta_2)m \\ \quad -\delta(\eta_3 u + N(d_0 - b_0))] + d_u \nabla^2 u, & \mathbf{x} \in \Omega, t > 0, \\ \frac{\partial m(\mathbf{x},t)}{\partial t} = \varepsilon\left(\frac{\beta u}{\alpha+u} - kNm\right) + d_m \nabla^2 m, & \mathbf{x} \in \Omega, t > 0, \\ \frac{\partial u(\mathbf{x},t)}{\partial \nu} = \frac{\partial m(\mathbf{x},t)}{\partial \nu} = 0, & \mathbf{x} \in \partial\Omega, t > 0, \\ u(\mathbf{x},0) = u_0(\mathbf{x}) \geq 0,\ m(\mathbf{x},0) = m_0(\mathbf{x}) \geq 0, & \mathbf{x} \in \Omega, \end{cases} \tag{2.4}$$

where $u(\mathbf{x}, t)$ and $m(\mathbf{x}, t)$ denote the density of cooperators and that of public goods in position $\mathbf{x}$ at time t, respectively; $\mathbf{x} \in \Omega \subseteq \mathbb{R}^2$ is a two-dimensional bounded domain; ν is the outward unit normal vector of the smooth boundary $\partial\Omega$; $\nabla^2 = \frac{\partial^2}{\partial x^2} + \frac{\partial^2}{\partial y^2}$ is the Laplacian operator; d_u and d_m are the diffusion coefficients for cooperators and public goods, respectively. The Neumann boundary conditions are employed in system (2.4) since individuals cannot leave and enter via the boundary. In the upcoming sections, we will investigate various dynamical properties of systems 2.3 and 2.4. This includes determining the presence and stability of equilibria, as well as identifying any instances of bistability, transcritical and Hopf bifurcations.

3 Dynamics of Temporal System

This section explores the various strategy dynamics properties, including the existence of equilibria, stability, bistability, transcritical bifurcation, and Hopf bifurcation for

the non-diffusion system (2.3), which helps to predict the outcome of the evolution of cooperation in conditions where individuals and public goods are well-mixed.

3.1 Existence of Equilibria

The two equilibria of system (2.3), namely $E_1(0, 0)$ and $E_2(N, \frac{\beta}{k(\alpha+N)})$, corresponding to the absence of cooperators and public goods, and the absence of defectors, respectively, always exist. Further, we explore the conditions under which the internal equilibrium $E^*(u^*, m^*)$ is feasible, enabling cooperators and defectors to coexist. From (2.3), u^* and m^* satisfy the following two equations:

$$(\eta_1 u^* + N\eta_2)m^* - \delta(\eta_3 u^* + N(d_0 - b_0)) = 0, \tag{3.1}$$

$$m^* = \frac{\beta u^*}{kN(\alpha + u^*)}. \tag{3.2}$$

Eliminating m^* by substituting (3.2) into (3.1), we have

$$\gamma_1 u^{*2} + \gamma_2 N u^* + N^2 \gamma_3 = 0, \tag{3.3}$$

where

$$\gamma_1 = \beta\eta_1 - N\delta k\eta_3,\ \gamma_2 = ((b_0 - d_0)N - \eta_3\alpha)k\delta + \beta\eta_2,\ \gamma_3 = \alpha\delta k(b_0 - d_0).$$

After solving Eq. (3.3), we obtain the solution

$$u^*_{\pm} = \frac{N\left(-\gamma_2 \pm \sqrt{\gamma_2^2 - 4\gamma_1\gamma_3}\right)}{2\gamma_1}. \tag{3.4}$$

Denote

$$\begin{aligned}
\hat{\eta}_3 &= \frac{\beta\eta_1}{N\delta k},\\
\eta^*_3 &= \frac{(b_0 - d_0)N}{\alpha} + \frac{\beta\eta_2}{k\alpha^2},\\
\tilde{\eta}_3 &= \frac{2\beta\eta_1 + (b_0 - d_0)Nk\delta + \beta\eta_2}{k\delta(2N + \alpha)},\\
\bar{\eta}_3 &= \frac{\beta(\eta_1 + \eta_2)}{k\delta(N + \alpha)} + (b_0 - d_0).
\end{aligned}$$

It is observed from (3.2) that $m^*_{\pm} > 0$ holds invariably. Therefore, the existence of $E^*_{\pm}$ only requires that $u^*_{\pm} \in (0, N)$ is guaranteed. Condition $u^*_{+} \in (0, N)$ holds if $\gamma_2^2 > 4\gamma_1\gamma_3$ and one of **(H1)**–**(H4)** below is true.
(H1): $\eta^*_3 < \eta_3 < \min\{\hat{\eta}_3, \tilde{\eta}_3, \bar{\eta}_3\}$.
(H2): $\eta_3 < \min\{\hat{\eta}_3, \tilde{\eta}_3, \bar{\eta}_3\}$ and $b_0 < d_0$.

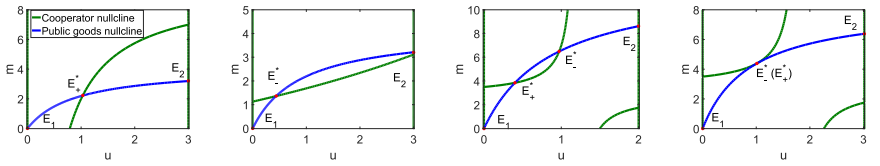

(a) E_1, E_2, and E_+^* exist (b) E_1, E_2, and E_-^* exist (c) E_1, E_2, E_-^*, and E_+^* exist (d) E_1, E_2, E_-^* (E_+^*) exist

Fig. 1 Existence of equilibria for system (2.3). The cooperator and the public goods nullclines are depicted by green and blue curves, respectively, obtained from $\frac{du}{dt} = 0$ and $\frac{dm}{dt} = 0$ of system (2.3). The equilibria marked with red dots are present at the intersection of the green and blue curves. Parameters: **a** $a_0 = 2.9$, $a_1 = 4$, $b_0 = 0$, $b_1 = 1$, $c_0 = 0.1$, $c_1 = 2$, $d_0 = 1$, $d_1 = 2$, $\delta = 2$, $\beta = 2.5$, $\alpha = 0.9$, $k = 0.2$, $N = 3$, $\varepsilon = 1$. **b** $a_1 = 3$, $b_0 = 2.3$. **c** $a_0 = 2$, $a_1 = 3$, $b_0 = 2$, $b_1 = 5$, $c_0 = 1$, $c_1 = 6$, $d_0 = 5$, $\delta = 7$, $N = 2$, $\beta = 5$. **d** $N = 3.0152$. Note that the remaining parameters of **b**, **c**, and **d** are taken from **a**. The values of the parameters are detailed in Table 3 (color figure online)

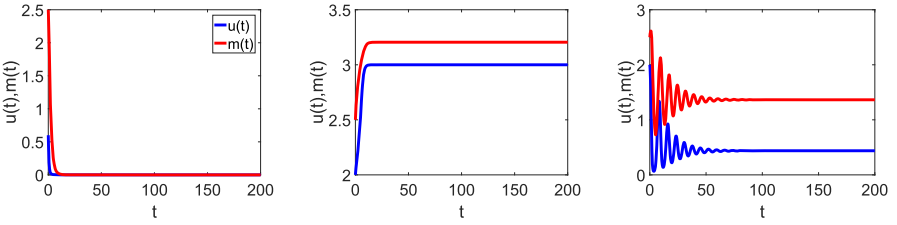

(a) E_1 is stable (b) E_2 is stable (c) E_-^* is stable

Fig. 2 Temporal behavior of cooperators and public goods for system (2.3). The blue and red curves depict the evolution of cooperators and public goods over time, respectively. The initial conditions for **a**, **b**, and **c** are (0.6, 2.5) and (2, 2.5), respectively. The parameters of **a** and **b** are $a_0 = 2.1$, $b_0 = 2.1$, $d_0 = 2.2$ and the rest of the parameters are adopted from Fig. 1b. The parameters of **c** remain the same as in Fig. 1b (color figure online)

(H3): $\max\{\hat{\eta}_3, \tilde{\eta}_3\} < \eta_3 < \eta_3^*$ and $b_0 < d_0$.
(H4): $\hat{\eta}_3 < \eta_3 < \min\{\tilde{\eta}_3, \bar{\eta}_3\}$.
Similarly, E_-^* exists i.e. $u_-^* \in (0, N)$ holds if $\gamma_2^2 > 4\gamma_1\gamma_3$ and one of **(H5)**–**(H8)** is satisfied.
(H5): $\eta_3^* < \eta_3 < \min\{\hat{\eta}_3, \bar{\eta}_3\}$ and $b_0 > d_0$.
(H6): $\max\{\tilde{\eta}_3, \bar{\eta}_3\} < \eta_3 < \hat{\eta}_3$ and $b_0 > d_0$.
(H7): $\eta_3 > \max\{\hat{\eta}_3, \eta_3^*, \bar{\eta}_3\}$ and $b_0 > d_0$.
(H8): $\max\{\hat{\eta}_3, \tilde{\eta}_3\} < \eta_3 < \min\{\eta_3^*, \bar{\eta}_3\}$.

In impoverished public goods environments, the disparities in payoffs between encounters among players employing different strategies and those among players employing the same strategy, along with the discrepancies in payoffs between encounters involving defectors, collectively contribute to determining the presence of internal equilibria. The existence of equilibria for system (2.3) is demonstrated in Fig. 1. The parameters for Fig. 1 are chosen to satisfy the above conditions for the existence of internal equilibria and to demonstrate the potential positioning of equilibria. The internal equilibrium points E_-^* and E_+^* coincide in Fig. 1d.

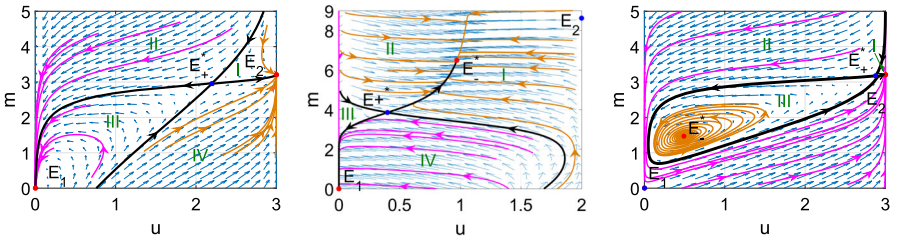

(a) E_1 and E_2 are stable (b) E_1 and E^*_- are stable (c) E_2 and E^*_- are stable

Fig. 3 Bistability of system (2.3). The phase portrait exhibits three different bistabilities. The red and blue dots mark the stable equilibria and saddle points, respectively. The black curves divide the plane into three or four regions. The magenta and yellow-brown lines from different positions converge to separate equilibria. The parameters in **a** and **b** are chosen from Figs. 2a and 1c, respectively. **c** $\delta = 2.11$ and the remaining parameters are selected from Fig. 2c (color figure online)

3.2 Local Stability and Bistability Analysis

For system (2.3), we investigate local stability and then derive bistability. Denote

$$\begin{aligned}
\varepsilon^* &= \frac{u^*_-}{kN^3}\left[((\eta_1-\eta_2)N-2\eta_1u^*)m^*_- + ((d_0-b_0-\eta_3)+2u^*_-\eta_3)\delta\right],\\
b_0^* &= \frac{1}{(\alpha+u^*_-)\delta kN^2}\Big[(((d_0-\eta_3)\delta + m^*_-(\eta_1-\eta_2))(\alpha+u^*_-)k-\beta\alpha\eta_2)N^2\\
&\quad +(2(\delta\eta_3-m^*_-\eta_1)(\alpha+u^*_-)k+\beta\alpha(\eta_1+\eta_2))u^*_-N-\beta\alpha u^{*2}_-\eta_1\Big],\\
\tilde{\varepsilon}^* &= \frac{u^*_+}{kN^3}\left[((\eta_1-\eta_2)N-2\eta_1u^*)m^*_+ + ((d_0-b_0-\eta_3)+2u^*_+\eta_3)\delta\right],\\
\tilde{b_0}^* &= \frac{1}{(\alpha+u^*_+)\delta kN^2}\Big[(((d_0-\eta_3)\delta + m^*_+(\eta_1-\eta_2))(\alpha+u^*_+)k-\beta\alpha\eta_2)N^2\\
&\quad +(2(\delta\eta_3-m^*_+\eta_1)(\alpha+u^*_+)k+\beta\alpha(\eta_1+\eta_2))u^*_+N-\beta\alpha u^{*2}_+\eta_1\Big].
\end{aligned}$$

The following theorem is utilized to elucidate the local stability of system (2.3).

Theorem 3.1 (I) *$E_1(0,0)$ is a locally asymptotically stable node if $d_0 > b_0$; $E_1(0,0)$ is a saddle point if $d_0 < b_0$.*

(II) *$E_2(N, \frac{\beta}{k(\alpha+N)})$ is a locally asymptotically stable node if $\delta(c_0-a_0) < \frac{\beta(\eta_1+\eta_2)}{k(N+\alpha)}$; $E_2(N, \frac{\beta}{k(\alpha+N)})$ is a saddle point if $\delta(c_0-a_0) > \frac{\beta(\eta_1+\eta_2)}{k(N+\alpha)}$.*

(III) *$E^*_-(u^*_-, m^*_-)$ is a locally asymptotically stable node or focus if $\varepsilon > \varepsilon^*$ and $b_0 > b_0^*$; $E^*_-(u^*_-, m^*_-)$ is an unstable node or focus if $\varepsilon < \varepsilon^*$ and $b_0 > b_0^*$; $E^*_-(u^*_-, m^*_-)$ is a saddle point if $b_0 < b_0^*$.*

(IV) *$E^*_+(u^*_+, m^*_+)$ is a locally asymptotically stable node or focus if $\varepsilon > \tilde{\varepsilon}^*$ and $b_0 > \tilde{b_0}^*$; $E^*_+(u^*_+, m^*_+)$ is an unstable node or focus if $\varepsilon < \tilde{\varepsilon}^*$ and $b_0 > \tilde{b_0}^*$; $E^*_+(u^*_+, m^*_+)$ is a saddle point if $b_0 < \tilde{b_0}^*$.*

Proof See "Appendix A". □

We discover the following bistability regarding system (2.3) by the discussion in "Appendix A".

Corollary 3.1 (I) $E_1(0,0)$ *and* $E_2(N, \frac{\beta}{k(\alpha+N)})$ *are stable when* $d_0 > b_0$ *and* $\delta(c_0 - a_0) < \frac{\beta(\eta_1+\eta_2)}{k(N+\alpha)}$.

(II) $E_1(0,0)$ *and* $E_-^*(u^*, m^*)$ *are stable when* $d_0 > b_0 > b_0^*$ *and* $\varepsilon > \varepsilon^*$.

(III) $E_2(N, \frac{\beta}{k(\alpha+N)})$ *and* $E_-^*(u_-^*, m_-^*)$ *are stable when* $\delta(c_0 - a_0) < \frac{\beta(\eta_1+\eta_2)}{k(N+\alpha)}$, $\varepsilon > \varepsilon^*$, *and* $b_0 > b_0^*$.

Choosing parameters that satisfy the local stability conditions of Theorem 3.1 yields Fig. 2, which illustrates the local stability of the temporal system. Three different evolutionary outcomes, including the extinction of cooperators and extremely poor public goods, pure cooperators and abundant public goods, and the coexistence of cooperators and defectors, occur due to different initial states and parameter values. For Fig. 2a and b, the same parameters are taken, but the difference in initial conditions leads to distinct evolutionary results. Keeping the initial value of the public goods fixed and increasing the initial density of cooperators leads to an evolutionary outcome from pure defectors to pure cooperators. Larger initial densities of cooperators enable pure cooperators to dominate if the initial concentration of public goods is identical. The third case of the Theorem 3.1 illustrated in Fig. 2c indicates that increasing the payoff of cooperator-defector encounters beyond its threshold and speeding up the evolution of public goods saves cooperators from extinction. The rapid turnover of public goods provides players with usable supplies, and the benefits to cooperators are increased, which motivates players to cooperate. Holding the initial values unchanged and varying the values of the parameters produce different evolutionary results see Fig. 2b and c.

The three types of bistability in the temporal system are depicted in Fig. 3, with parameters chosen based on Corollary 3.1. Illustrating the first case of the Corollary 3.1 Fig. 3a shows that if the initial values are taken from regions II and III (resp. I and IV), the densities finally converge to E_1 (resp. E_2). Thus, if the initial density of cooperators is fixed, high initial concentrations of public goods lead to the extinction of cooperators and if the initial quantity of public goods is kept fixed, then the likelihood of cooperators survival is a non-decreasing function of the initial density of cooperators. Therefore, barren initial public goods and high initial values for the cooperator facilitate the survival and continuation of cooperators. Illustrating the second case of the Corollary 3.1 Fig. 3b displays two stable equilibria E_1 and E_-^*. The basins of attraction for E_1 (resp. E_-^*) are regions III and IV (resp. I and II). Under such circumstances, a high initial density of cooperators or an adequate supply of public goods assists the cooperators in escaping extinction. Illustrating the third case of the Corollary 3.1 Fig. 3c depicts two stable equilibria E_2 and E_-^*. If initial densities of public goods and cooperators belong to region III (resp. regions I and II) then densities eventually converge to E_-^* (resp. E_2). After a prolonged period of evolution, cooperators and defectors eventually achieve stable coexistence when the population initially resides in a moderate concentration of public goods. Various evolutionary consequences can occur in the same subgraph with the same parameters due to varying initial states. Comparing the three subgraphs, we find that even with the same initial values different parameters might lead to diverse evolutionary outcomes. Therefore,

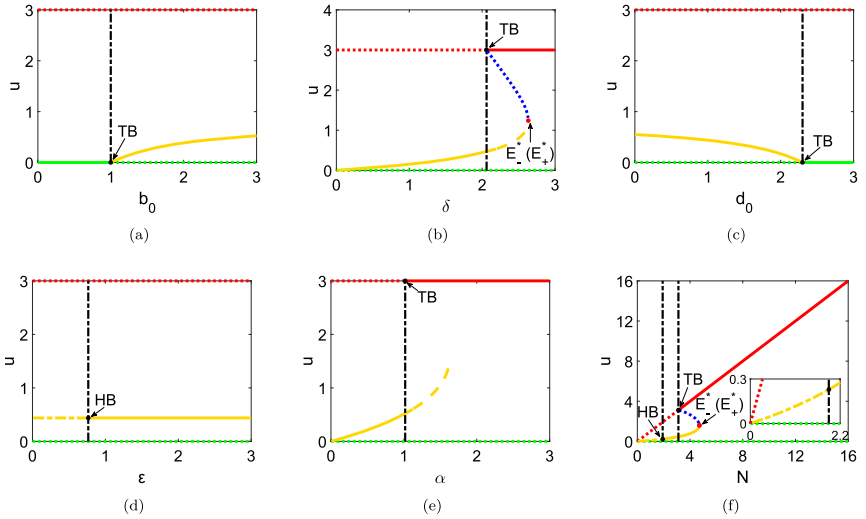

Fig. 4 Stability of equilibria and bifurcation depending on b_0, δ, d_0, ε, α, and N for system (2.3). The green, red, blue, and yellow lines indicate the values of u for E_1, E_2, E_+^*, and E_-^*, respectively. The solid, dotted, dashed, and dash-dotted lines depict stable equilibria, saddle points, unstable focus, and the emergence of periodic solutions, respectively. The HB and TB marked by solid black dots indicate the Hopf and transcritical bifurcations, respectively. The black dash-dotted line indicates the threshold at which bifurcation happens. The parameters and initial values remain unchanged from those in Fig. 2c. Bistability occurs in intervals $\delta \in (2.0604, 2.1967)$, $\alpha \in (1.0179, 1.1242)$ and $N \in (3.1179, 4.7079)$. Some calculations yield critical values $\delta^* = 2.0604$ and $\varepsilon^* = 0.7653$ (color figure online)

the choice of parameter values, the initial density of cooperators, and the initial state of the public goods can all lead to multiple evolutionary outcomes. In situations of scarce public goods, individuals within the population necessitate more of them to sustain essential life characteristics. This circumstance demands a high density of cooperators to facilitate the production of public goods. This explains the initial high density of cooperators favoring the continuation of cooperation in the case of initial public goods scarcity.

3.3 Bifurcation Analysis

In this subsection we explore the transcritical and Hopf bifurcations for system (2.3).

Theorem 3.2 (I) *If $d_0 = b_0$, then a transcritical bifurcation appears at $E_1(0, 0)$.*
(II) *If $\delta = \delta^*$, then a transcritical bifurcation appears at $E_2(N, \frac{\beta}{k(\alpha+N)})$.*
(III) *If $\varepsilon = \varepsilon^*$ and $b_0 > b_0^*$, then a Hopf bifurcation appears at $E_-^*(u_-^*, m_-^*)$.*

Proof See "Appendix B". □

Following the discussion above, we know that the Hopf bifurcation occurs at $E_-^*(u_-^*, m_-^*)$. However, the characteristics of the Hopf bifurcation such as direction and stability have not been clarified. Next, for the Hopf bifurcation, we investigate its

Table 1 The existence of equilibria, stability, and bifurcations for the temporal system (2.3)

Equilibrium	Existence	Stable	Saddle point	Unstable node or focus	Bifurcation
$E_1(0,0)$	Always	$d_0 > b_0$	$d_0 < b_0$	–	TB, $d_0 = b_0$
$E_2(N, \frac{\beta}{k(\alpha+N)})$	Always	$\delta(c_0 - a_0) < \frac{\beta(\eta_1+\eta_2)}{k(N+\alpha)}$	$\delta(c_0 - a_0) > \frac{\beta(\eta_1+\eta_2)}{k(N+\alpha)}$	–	TB, $\delta = \delta^*$
$E_-^*(u_-^*, m_-^*)$	(H1)–(H4)	$\varepsilon > \varepsilon^*$ and $b_0 > b_0^*$	$b_0 < b_0^*$	$\varepsilon < \varepsilon^*$ and $b_0 > b_0^*$	HB, $\varepsilon = \varepsilon^*$, $b_0 > b_0^*$
$E_+^*(u_+^*, m_+^*)$	(H5)–(H8)	$\varepsilon > \tilde{\varepsilon}^*$ and $b_0 > \tilde{b_0}^*$	$b_0 < \tilde{b_0}^*$	$\varepsilon < \tilde{\varepsilon}^*$ and $b_0 > \tilde{b_0}^*$	–

TB and HB denote transcritical bifurcation and Hopf bifurcation, respectively

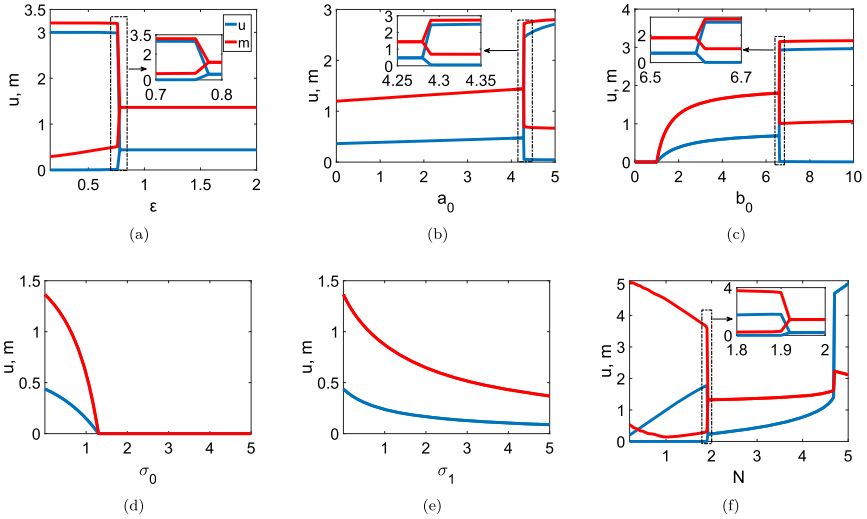

Fig. 5 The dependence of cooperators and public goods in system (2.3) on parameters ε, a_0, b_0, σ_0, σ_1, and N. **a** System (2.3) is unstable at E^*_- when $\varepsilon < 0.7653$ and is stable at E^*_- when $\varepsilon \in (0.7653, 2)$. Hopf bifurcation occurs if $\varepsilon = 0.7653$. **b** System (2.3) is stable at E^*_- when $a_0 < 4.2905$ and is unstable at E^*_- when $a_0 \in (4.2905, 5)$. Hopf bifurcation occurs if the payoff when the cooperators meet is equal to 4.2905. **c** E_1 is stable when $b_0 < 1$. If b_0 lies in the interval $(1, 6.6)$,then E^*_- is stable. E^*_- is unstable and the periodic solution occurs when $b_0 \in (6.6, 10)$. Transcritical and Hopf bifurcations occur at $b_0 = 1$ and $b_0 = 6.6$, respectively. **d** E^*_- is stable when $\sigma_0 < 1.3$. E_1 is stable if σ_0 lies in the interval $(1.3, 5)$. The transcritical bifurcation arises at $\sigma_0 = 1.3$. **e** E^*_- is stable. **f** Periodic solutions appear when $N < 1.9225$. E^*_- is stable if N lies in the interval $(1.9225, 4.7079)$. If $N \in (4.7079, 5)$, then E_2 is stable. The remaining parameter values are taken from Fig. 2c except for those shown in this figure (color figure online)

direction and stability. We know that Υ determines the direction of the Hopf bifurcation from "Appendix C". The Hopf bifurcation is subcritical (supercritical) if $\Upsilon < 0$ ($\Upsilon > 0$). $S_1(\varepsilon^*)$ determines the stability of the periodic solution. The periodic solution is stable (unstable) if $S_1(\varepsilon^*) < 0$ ($S_1(\varepsilon^*) > 0$). The direction of the Hopf bifurcation and the stability of the periodic solutions depend on $S_1(\varepsilon^*)$ since $\varphi'(\varepsilon^*) < 0$. Here, the forward and backward bifurcations are subcritical and supercritical bifurcations, respectively. Thus, we conclude with Theorem 3.3.

Theorem 3.3 *Suppose $\varepsilon > \varepsilon^*$ and $b_0 > b_0^*$. Hopf bifurcation is subcritical (resp. supercritical), and the periodic solution is stable (resp. unstable) if $S_1(\varepsilon^*) < 0$ (resp. $S_1(\varepsilon^*) > 0$).*

Density of strategy C presents different evolutionary trends with parameters b_0, δ, d_0, ε, α, and N (see Fig. 4). Increasing the values of payoff of cooperator encounter defector under poor public goods conditions (b_0), baseline payoffs (α), relative timescale (ε), and player density (N) enhances the ability of cooperators to survive. However, increasing the value of defector–defector payoff under scarce public goods conditions (d_0) leads to the extinction of cooperators. Interestingly, there is more than one parameter causing the bifurcation and bistability. Table 1 presents the properties of equilibria and bifurcations for the temporal system. In Fig. 4a, E_1 is stable, and E^*_- does not

exist when $b_0 < d_0$. If $b_0 > d_0$, E_-^* exists and is stable, while E_1 becomes a saddle point. The transcritical bifurcation occurs at $b_0 = d_0$, which corresponds to Theorem 3.2 (I). In addition, under given conditions E_2 is always a saddle point meaning that the value of b_0 does not affect the stability of E_2. There is an overall upward trend in the density of cooperators as b_0 increases, which means that increasing the payoff of strategy C when it meets strategy D inspires more players to pursue strategy C.

The second case of Theorem 3.2 is illustrated in Fig. 4b. It shows that E_-^* is stable, while E_2 is a saddle point if $\delta < \delta^*$ and E_2 remains stable when $\delta > \delta^*$, the transcritical bifurcation occurs at $\delta = \delta^*$. The interesting bistable phenomenon emerges due to δ. Evidently, the value of δ does not affect the stability of E_1, which complies with Theorem 3.1 (I). The small δ favors the prevalence of the cooperative strategy in the population. Once the critical value δ^* is reached, defectors become extinct, and cooperators dominate.

Illustrating the first case of the Theorem 3.2 Fig. 4c shows the occurrence of transcritical bifurcation at $d_0 = b_0$. Notice that the density of strategy C decreases with increasing d_0 until d_0 equals b_0. If d_0 is greater than b_0, no player in the population adopts strategy C, and strategy D dominates. This suggests that increasing defector payoffs during defector encounters weakens players' incentive to adopt strategy C. Once the defector's payoff exceeds the threshold, no player is happy to adopt strategy C, which is detrimental to the continuation of the cooperative strategy.

Figure 4d reveals the effect of relative timescale ε on the evolution of strategy C. It demonstrates that E_1 and E_2 are always saddle points and are unaffected by relative timescale changes. Interestingly, the periodic solution appears when $\varepsilon < \varepsilon^*$. In this case, the density of cooperators is in a state of periodic oscillation as shown in Fig. 6c and d. This cyclical oscillatory behavior offers further possibilities for the retention of biodiversity. The oscillating state gives both strategies C and D a fair chance of survival. The Hopf bifurcation occurs when $\varepsilon = \varepsilon^*$, which verifies the third case of Theorem 3.2. Once $\varepsilon > \varepsilon^*$, the density of cooperators is no longer influenced by ε. If public goods evolve at a faster rate, the evolutionary outcomes of strategies in populations no longer depend on relative timescales.

To explore the role of the saturation parameter of production, we plot the variation in the density of strategy C with α in Fig. 4e. When α lies in the bistable interval of α, E_2 and E_-^* are locally stable, and evolutionary outcomes are contingent on the initial values of strategy densities and public goods. As the α increases, the density of cooperators in stable equilibrium E_-^* rises, while after transcritical bifurcation occurs, E_2 becomes stable. In this case, the increase in cooperators is more pronounced when the small α gradually increases. When the value of production saturation reaches the threshold, the cooperators fill the entire population, and the defectors vanish.

We examine the effect of total player density N in Fig. 4f. While N is changing between 0 and the first threshold periodic solutions occur, where cooperators and defectors oscillate and coexist. When N reaches the first threshold, system (2.3) has a Hopf bifurcation at E_-^*. When N reaches the second threshold, E_2 transitions from a saddle point to a stable equilibrium, and a transcritical bifurcation emerges. System (2.3) exhibits a bistability, which is embodied in the fact that E_2 and E_-^* are stable when N lies in its bistable interval. When N exceeds the bistable interval, E_2 is stable, and E_-^* is absent. When fewer actors are involved in the game, individuals will vacillate

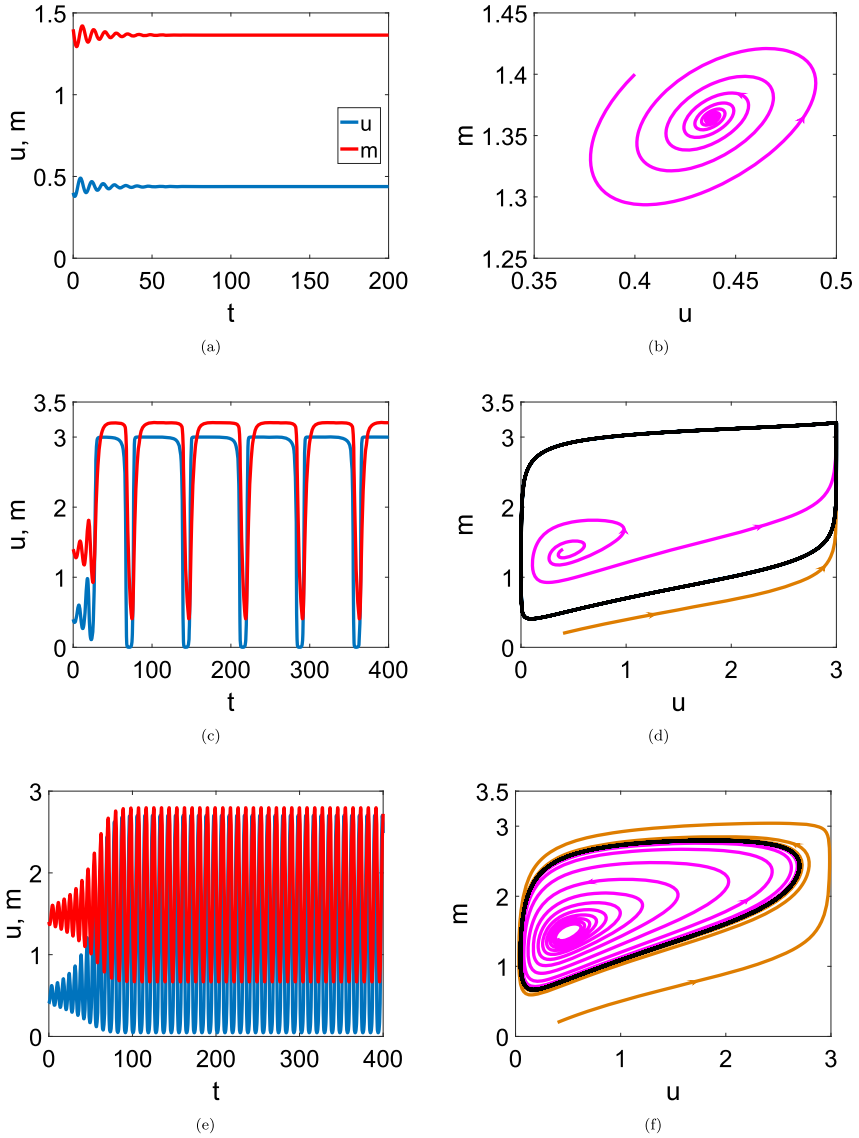

Fig. 6 Temporal evolution of strategy C and public goods (on the left), and phase trajectories in the um-plane (on the right). **a**, **b** E_{-}^{*} is stable. **c**, **d** Choose $\varepsilon = 0.5$ and a stable periodic solution occurs near the unstable equilibrium E_{-}^{*}. **e**, **f** Setting $a_0 = 4.95$ yields that E_{-}^{*} is unstable, and a stable periodic solution appears (color figure online)

between strategies C and D, leading to circular choices. With an increasing density of players and heightened competition, individuals exhibit a distinctive shift in their choice of strategies, manifested in a phenomenon of bistability. In situations with a high density of players, supplies become insufficient, prompting individuals to lean towards cooperation to survive.

The changes in public goods and density of strategy C with ε, a_0, b_0, σ_0, σ_1, and N are depicted in Fig. 5. While relative timescale value is small enough ($\varepsilon < \varepsilon^*$), strategy C and public goods oscillate between the upper and lower lines, indicating the emergence of periodic solutions. Some calculations give $S_1(\varepsilon^*) < 0$. Thus, it follows from Theorem 3.3 that the periodic solution is stable and the Hopf bifurcation is subcritical. More detailed information on the periodic solution due to relative timescale value is available in Fig. 6. Dencity of strategy C and public goods ultimately oscillate in cycles as time changes and the periodic solution is stable. The Hopf bifurcation appears when $\varepsilon = \varepsilon^*$ corresponding to the information expressed in Fig. 4d. The parameters ε and a_0 for Fig. 6a and b are taken from the stable interval in Fig. 5. Figure 6a and b illustrate the stabilization of system (2.3) at E_-^*. A Hopf bifurcation occurs at $a_0 = 4.2905$. System (2.4) is stable at E_-^* when $a_0 \in (0, 4.2905)$. Once the payoff when the cooperators encounter each other exceeds its threshold, E_-^* becomes unstable, and stable periodic solutions emerge. The transition of stability due to the change of b_0 is demonstrated in Fig. 5c. The system is stable at $E_1(0, 0)$ when b_0 lies in interval $(0, 1)$. As b_0 increases, the system is stable at the internal equilibrium E_-^*. Then, E_-^* becomes unstable, and periodic solutions appear when $b_0 > 6.6$. Figure 5d and e inspect the effects of cooperation costs σ_0 and σ_1 on the evolution of cooperators and public goods. The transcritical bifurcation emerges at $\sigma_0 = 1.3$, which allows $d_0 = b_0$ to hold, thus verifying Theorem 3.2(I). Unsurprisingly, raising the cost of cooperative strategies discourages individuals from choosing to cooperate. In Fig. 5f, changes in N lead to multiple shifts in stability. Periodic solutions appear near the internal equilibrium E_-^* if $N < 1.9225$. When N exceeds its threshold, the stability of the internal equilibrium E_-^* changes, transitioning from unstable to stable. After $N = 4.7079$, the stability shifts once more, from the internal equilibrium E_-^* being stable to E_2 being stable.

We next scrutinize the combined effect of the two parameters on the eco-evolutionary outcome. In Fig. 7, the shades of color indicate the evolutionary outcome of strategy C and public goods, forming heat maps. We compare the effects of the poverty and richness payoff matrices on evolution in Fig. 7a–l. We explore the far-reaching implications of the different payoffs when cooperators encounter each other in barren and abundant public goods settings as shown in Fig. 7a–d. If the cooperators meet in a poverty public goods, then the increase in the payoff for cooperators is conducive to the evolution of the cooperators in a positive direction. However, the increase in the density of cooperators is relatively slight. Surprisingly, a_1 causes the huge transition of the densities, regardless of the size of a_0. In other words, when players employing strategy C meet in an abundance of public goods, the higher payoffs contribute to populations filled with cooperators. We discover that changes in a_1 have a more significant and more profound impact on the evolution of cooperators and public goods than does a_0. The region III of the first row of Fig. 7 shows relatively significant differences in densities between (a) and (b), (c) and (d) meaning that the amplitude

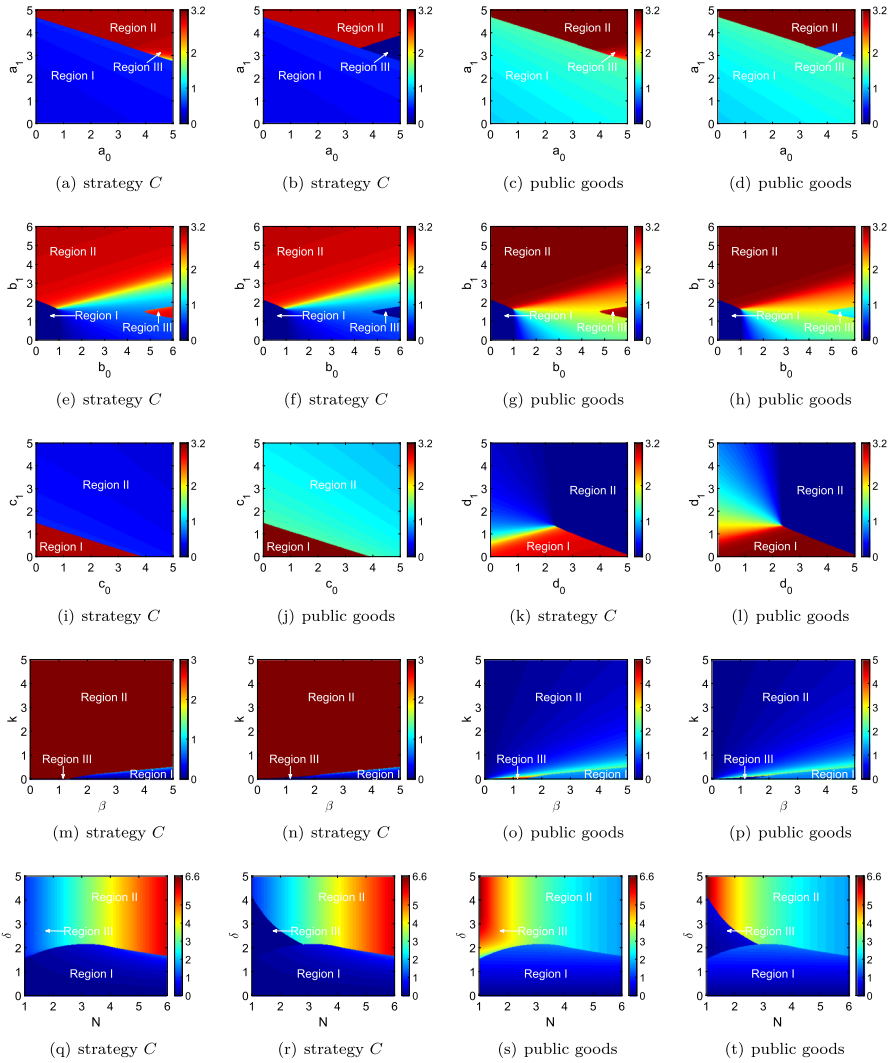

(a) strategy C (b) strategy C (c) public goods (d) public goods

(e) strategy C (f) strategy C (g) public goods (h) public goods

(i) strategy C (j) public goods (k) strategy C (l) public goods

(m) strategy C (n) strategy C (o) public goods (p) public goods

(q) strategy C (r) strategy C (s) public goods (t) public goods

Fig. 7 Evolutionary outcomes of cooperative strategies and public goods induced by two-dimensional parameters. **a**–**d**, **m**–**t** Stable E^*_-, stable E_2, and unstable E^*_+ are located in regions I, II, and III, respectively. **e**–**h** Stable E_1, stable E^*_-, and unstable E^*_+ are located in regions I, II, and III, respectively. **i**, **j** The stable E_2 and E^*_+ are located in regions I and II, respectively. **k**, **l** The stable E^*_+ and E_1 are located in regions I and II, respectively. Note that periodic solutions occur in Region III. Region III in the first and second columns represents the maximum and minimum values for the density of strategy C, respectively. Region III in the third and fourth columns denotes the maximum and minimum values for public goods, respectively. Parameters are taken from Fig. 2c (color figure online)

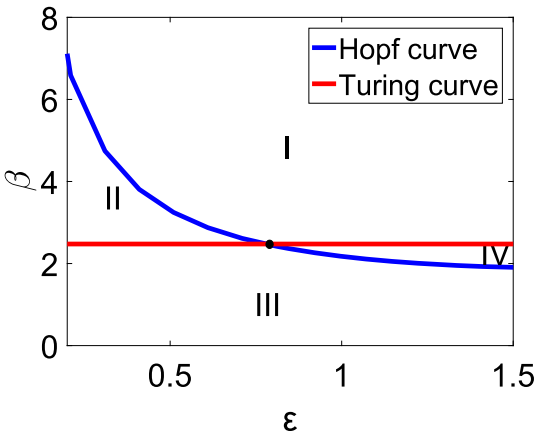

Fig. 8 Turing–Hopf bifurcation diagram in the plane ε-β. The Turing–Hopf bifurcation occurs at the black point $(\beta^*, \varepsilon^{**}) = (2.476, 0.762)$ (color figure online)

of the oscillations in the density of cooperators and the concentration of public goods is substantial, and this property is also revealed in Figs. 5b and 6e. A large a_0 and an intermediate value of a_1 allow cooperators, defectors, and public goods to vary within a specific range.

Figure 7e–h compares the effects of cooperators' payoffs on the strategies selected by players and the evolution of public goods in barren and rich environments when cooperators and defectors encounter each other. When b_1 is small, an increase in b_0 favors strategy C to dominate. Unexpectedly, when b_1 is big reducing the value of b_0 stimulates the players to choose the cooperative strategy. Similar to before, in region III of the second row of Fig. 7, system (2.3) oscillates around E_-^*, which gives defectors the possibility to occupy the population. A big b_1 is always beneficial for cooperators and public goods, regardless of the size of b_0. When cooperators and defectors meet, the high payoffs of cooperators always contribute positively to strategy C in a rich environment. In contrast, the high payoffs for cooperators in poor environments have sometimes been detrimental to the continuation of strategy C. The reason for this phenomenon is that the abundance of the public goods exceeds the δ, and the payoff matrix of the poor public goods plays a negative role, in which case individuals receive lower payoffs in favor of survival.

To probe the effect of defectors' payoffs on the evolution of players and public goods when defectors encounter cooperators and defectors, respectively we plot heat maps for c_0 and c_1, d_0 and d_1 in Fig. 7i–l. In Fig. 7i and j, it can be observed that small c_0 and c_1 enable a high density of cooperators in the population. Under this scenario, defectors are extinct, and public goods are supremely abundant. If c_1 is small, the density of strategy C first remains at its highest level as c_0 increases. Once the switch from region I to region II is made, then increasing c_0 causes the density of strategy C to decrease. Similarly, when c_0 is small, increasing the value of c_1 within a small range does not affect the absolute dominance of strategy C. Increasing c_1 will only hurt the cooperators and the public goods once conversion from region I to region II has taken place.

An attractive phenomenon appears in Fig. 7k and l. When d_1 is small, an increase in d_0 within a specific range is advantageous for cooperators and public goods, but an excessive increase in d_0 is counterproductive, causing the cooperators to become extinct and the public goods to be depleted. When d_1 is big, decreasing d_0 provides a relatively small benefit to both cooperators and public goods. This illustrates that cooperators depend more on small d_0. Figure 7k and l also indicate that cooperators and public goods prefer small d_1. Abundant public goods amplify changes in the fitness of cooperators and defectors caused by changes in payoffs. The replicator equation is distinguished by the fact that strategies with higher fitness are popular with players in the population. In Fig. 7a–l, the color changes more dramatically in the vertical direction than in the horizontal direction. Therefore, the evolutionary outcomes of strategies and public goods are more sensitive to players' payoffs under rich public goods than under poor public goods conditions.

The transformation from the region I to region II in Fig. 7m–p discloses that an increase in the consumption rate of public goods increases the likelihood of survival of cooperators. When k is small, the fascinating phenomenon emerges that increase in β does not favor the dominance of cooperators. Unsurprisingly, reducing consumption rates and increasing maximum productivity can enrich public goods. Those figures also illustrate that the dominance of cooperators not necessarily leads to abundant public goods.

In Fig. 7q–t, when δ is small the increase in the density of players involved in the game brings a minor benefit for the cooperators. When δ is large, this correlation becomes more pronounced. When δ is big, increasing the player density benefits cooperation and makes the public goods more barren. In addition, we note an interesting phenomenon in region II, the size of delta after fixing the density of participants in the game does not affect the evolution of cooperators and public goods.

4 Dynamics of Diffusion System (2.4)

In this section, we explore relevant properties of diffusion system (2.4), such as local stability, Turing instability, Hopf bifurcation, and Turing–Hopf Bifurcation.

4.1 Local Stability

Denote $b_0^{**} = \frac{\eta_1(1-2u^*m^*)-\eta_2}{\delta N} + \frac{2u^*\eta_3}{N} - \eta_3 + d_0$ and $\hat{b}_0 = \frac{1}{u^*+N}\left[u^*\eta_2 - N(d_1 - b_1 - d_0)\right]$. For system (2.4), we summarize the stability of steady states $E_1(0,0)$, $E_2(N, \frac{\beta}{k(\alpha+N)})$, and $E_-^*(u_-^*, m_-^*)$ using the following theorem.

Theorem 4.1 (I) *The steady state $E_1(0,0)$ is spatially stable if $d_0 > b_0$; while $E_1(0,0)$ is spatially unstable if $d_0 < b_0$.*

(II) *The steady state $E_2(N, \frac{\beta}{k(\alpha+N)})$ is spatially stable if $\delta(c_0 - a_0) < \frac{\beta(\eta_1+\eta_2)}{k(N+\alpha)}$; while $E_2(N, \frac{\beta}{k(\alpha+N)})$ is spatially unstable if $\delta(c_0 - a_0) > \frac{\beta(\eta_1+\eta_2)}{k(N+\alpha)}$.*

(III) *The steady state $E_-^*(u_-^*, m_-^*)$ is spatially stable if $b_0 > \max\{b_0^*, b_0^{**}\}$ or $b_0^{**} < b_0 < \hat{b}_0$.*

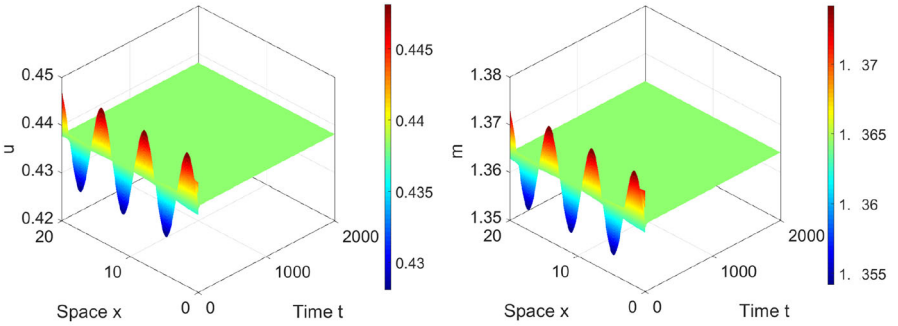

(a) cooperators (b) public goods

Fig. 9 Evolution of cooperators and public goods over time t and space x. The solution tends to E_-^* when $\varepsilon = 1 > \varepsilon^{**} = 0.7603$. The initial densities and parameters are $u(x, 0) = 0.4381 + 0.01\sin x$, and $m(x, 0) = 1.3642 + 0.01\sin x$, and $\varepsilon = 1$, $a_1 = 2.9$, $a_1 = 3$, $b_0 = 2.3$, $b_1 = 1$, $c_0 = 0.1$, $c_1 = 2$, $d_0 = 1$, $d_1 = 2$ $\delta = 2$, $\beta = 2.5$, $\alpha = 0.9$, $k = 0.2$, $N = 3$, $d_u = 2$, $d_m = 3$ (color figure online)

Proof See "Appendix D". □

4.2 Turing Instability

Next, we derive the conditions for Turing instability. According to "Appendix E", we obtain Theorem 4.2 as follows.

Theorem 4.2 *Suppose* $\varepsilon > \varepsilon^*$ *and* $b_0 > b_0^*$. *If* $\frac{d_m}{d_u} > \phi_1$, *then the Turing instability driven by diffusion appears near the steady state* $E_-^*(u_-^*, m_-^*)$.

Theorem 4.2 reveals that the diffusion ratio (d_m: d_u) of public goods and cooperators is decisive for whether Turing instability occurs. Smaller diffusion ratios do not affect the stability of the steady state $E_-^*(u_-^*, m_-^*)$, while larger diffusion ratios destabilize the steady state $E_-^*(u_-^*, m_-^*)$, and Turing instability arises.

4.3 Hopf Bifurcation

The diffusion system (2.4) undergoes a Hopf bifurcation as described in Theorem 4.3 below.

Theorem 4.3 *The diffusion system* (2.4) *undergoes Hopf bifurcation at* $\varepsilon = \varepsilon^{**}$ *if* $\varepsilon^{**} > \frac{j_{11}^* d_m}{N k d_u}$ *and* $b_0 > b_0^*$.

Remark. The periodic solution is spatially homogeneous if $n = 0$. The periodic solution is spatially non-homogeneous if $n \neq 0$.

Proof See "Appendix F". □

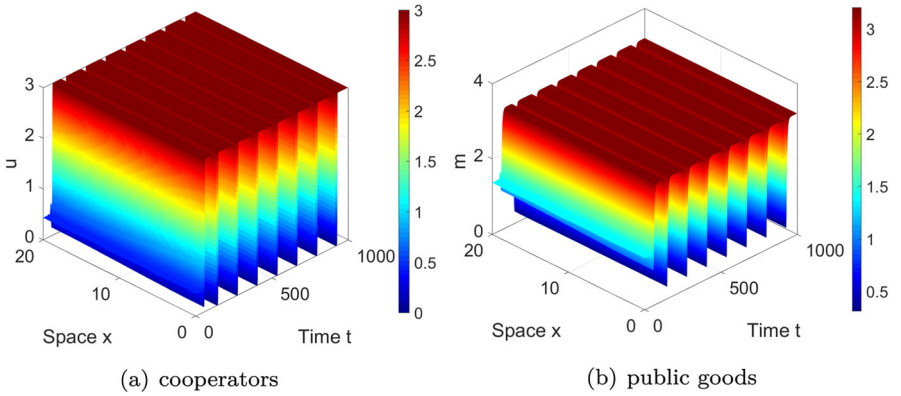

(a) cooperators (b) public goods

Fig. 10 Evolution of cooperators and public goods over time t and space x. The stable time-periodic solution appears when $\varepsilon = 0.35 < \varepsilon^{**} = 0.7603$ (color figure online)

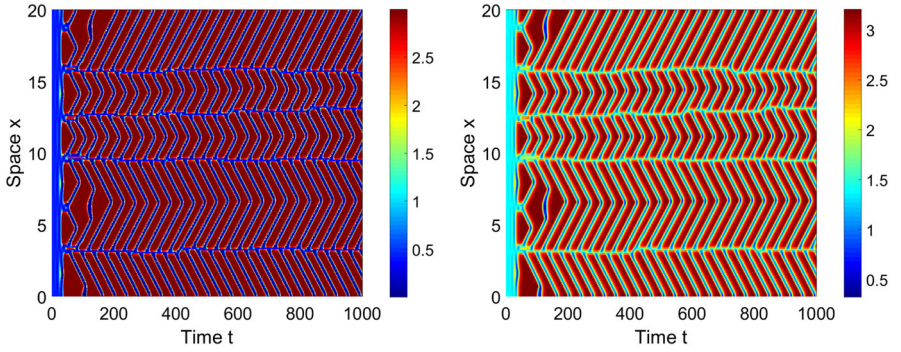

(a) cooperators (b) public goods

Fig. 11 Evolution of cooperators and public goods over time t and space x. Unstable spatially non-homogeneous periodic solution emerges (color figure online)

4.4 Turing–Hopf Bifurcation

Next, we explore the existence of the Turing–Hopf bifurcation. According to "Appendix G", we obtain Theorem 4.4 as follows.

Theorem 4.4 *Suppose that* $d_u < \hat{d}_u$ *and* $\eta_2 < \frac{\eta_1 u^*}{N}$, *then system* (2.4) *undergoes a Turing–Hopf bifurcation at point* $(\beta, \varepsilon) = (\beta^*, \varepsilon^{**})$.

Figs. 8, 9, 10 and 11 illustrate Turing–Hopf bifurcation, whose conditions are formulated in Theorem 4.4. The parameters for those figures are chosen from Fig. 2c to allow the comparison between the temporal and diffusion systems and to explore the impact of diffusion on the evolution of cooperation. Table 2 provides a summary of the conditions that lead to steady states stability and the emergence of Turing–Hopf bifurcations. In Figs. 5a and 12, Hopf bifurcations occur at ε^* and ε^{**}, respectively, meaning that the spatially diffusive system (2.4) has an earlier Hopf bifurcation than the non-diffusive system (2.3).

Table 2 Spatial stability and Turing–Hopf bifurcation for the diffusion system 2.4

Steady state	Spatially stable	Spatially unstable	Turing–Hopf bifurcation
$E_1(0,0)$	$d_0 > b_0$	$d_0 < b_0$	–
$E_2(N, \frac{\beta}{k(\alpha+N)})$	$\delta(c_0 - a_0) < \frac{\beta(\eta_1+\eta_2)}{k(N+\alpha)}$	$\delta(c_0 - a_0) > \frac{\beta(\eta_1+\eta_2)}{k(N+\alpha)}$	–
$E_-^*(u_-^*, m_-^*)$	$b_0 > \max\{b_0^*, b_0^{**}\}$ or $b_0^{**} < b_0 < \hat{b}_0$	–	$d_u < \hat{d}_u, \eta_2 < \frac{\eta_1 u_-^*}{N}, (\beta, \varepsilon) = (\beta^*, \varepsilon^{**})$

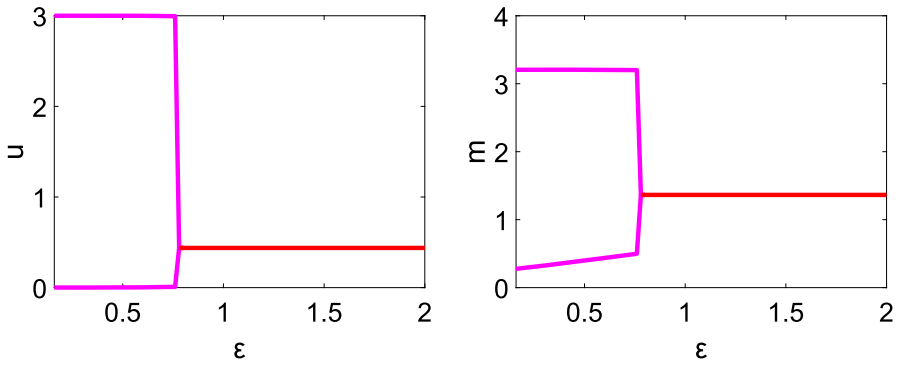

(a) cooperators (b) public goods

Fig. 12 The dependence of cooperative strategies and public goods in system (2.4) on parameter ε. Hopf bifurcation appears when $\varepsilon = \varepsilon^{**} = 0.7603$ (color figure online)

The Turing and Hopf bifurcation curves depicted in Fig. 8 divide the plain into four regions. Figure 9 illustrates that if parameters of system (2.4) correspond to region I of Fig. 8, solution eventually converges to stable state E_-^*, which indicates that the stability of the constant steady state E_-^* is not affected by ε when $\varepsilon > \varepsilon^{**}$. If parameters of the system (2.4) belong to region II of Fig. 8, the stable time-periodic solution emerges as depicted in Fig. 10. The values of parameters belonging to region III meet the requirements stated in Theorem 4.4. Hence, E_-^* is Turing–Hopf unstable, and unstable spatially heterogeneous periodic solutions appear, as shown in Fig. 11.

5 Pattern Formation and Chaos

In this section, we further investigate the effects of parameters and diffusion coefficients on the spatial distribution of players and public goods. Figures 13, 14, 15, 16, 17 and 20 contain stationary and chaotic patterns, with the spatial patterns of cooperators and public goods evolving over time, showing various spatial distributions. To enable comparison the evolution of cooperation in well-mixed and heterogeneous environments, the parameters in Figs. 13, 14, 15, 16, 17, 18, 19, 20, 21 and 22 are chosen from Fig. 2c.

5.1 Pattern Formation Due to Relative Timescale

The different values of the time scale ε bring about several Turing patterns. In the first column of Fig. 13, when public goods evolve slower than strategies ($\varepsilon < 1$), the cooperators mainly cluster at the circular closed stripes, and a few are located in the vicinity of the circular closed stripes in the form of spots or short stripes. The predominance of cooperators at the higher abundance of public goods indicates that the abundance of public goods helps cooperators to survive and reproduce. The shape of the spatial distribution of public goods is relatively similar to that of the spatial

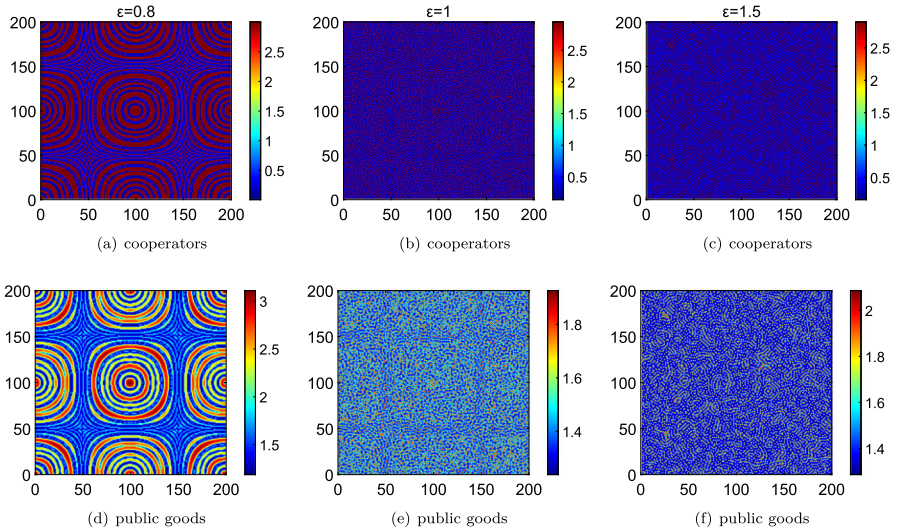

Fig. 13 Spatial distribution of cooperators and public goods with $\varepsilon = 0.8$ (column I), $\varepsilon = 1$ (column II), and $\varepsilon = 1.5$ (column III). The initial heterogeneous perturbation $u(x, y, 0) = u^\star + 0.01\cos\frac{2\pi x}{200}\cos\frac{2\pi y}{200}$, $m(x, y, 0) = m^\star + 0.01\cos\frac{2\pi x}{200}\cos\frac{2\pi y}{200}$ is performed on the homogeneous steady state $(u^\star, m^\star)$, with the spatial domain $[0, 200] \times [0, 200]$. All parameters are taken from Fig. 2c except for those mentioned deliberately and those shown in the figures. The values of the diffusion coefficients d_u and d_m are 0.1 and 3, respectively (color figure online)

distribution of cooperators, both showing circular closed stripes, the difference being that the density of public goods is not consistent, compared to that of cooperators. It illustrates that cooperators do not require extremely high densities of public goods and that as long as public goods are not particularly scarce, there is hope for cooperators to survive. As shown in the second column of Fig. 13, increasing the evolution rate of public goods to that of strategies ($\varepsilon = 1$) results in a shift in the spatial distribution of cooperators from circular stripes to scattered spots and short stripes. In this case, cooperators are less capable of aggregating than they are under conditions of slow public goods evolution rate. Further increasing of the evolution rate of public goods makes it faster than the speed of the game ($\varepsilon > 1$). The third column of Fig. 13 illustrates, that high relative timescale value brings about a sparser distribution of cooperators and public goods. Thus, large time scales are not conducive to the density of cooperators and public goods. For the temporal system, we know that increasing the timescale does not affect the evolutionary outcome when the relative timescale exceeds its threshold value. However, increasing the value of the relative timescale decreases the cohesion and survival chances of the cooperators, for the diffusion system.

5.2 Pattern Formation Due to Density of Players

We now explore the effect of the total density of players N on the Turing pattern of cooperators and public goods. For the two-player game in column I of Fig. 14, some

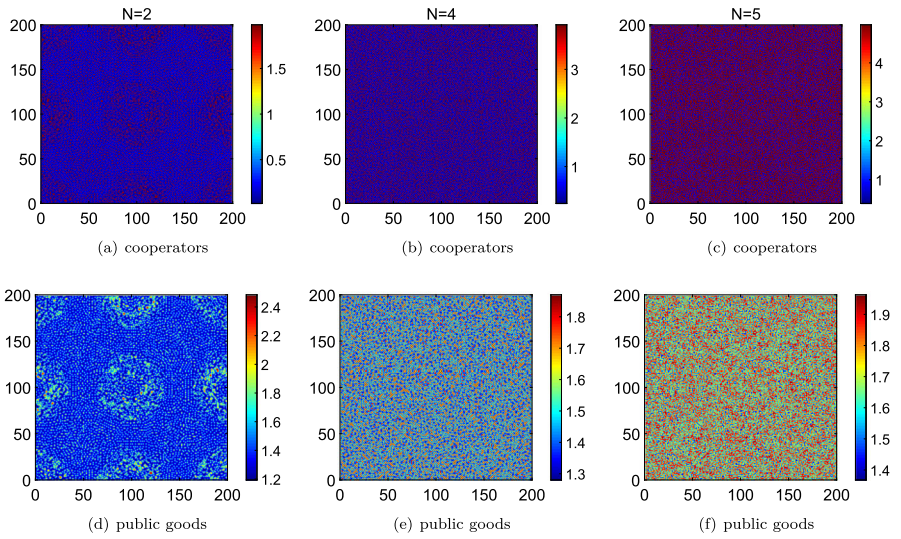

Fig. 14 Spatial distribution of cooperators and public goods with $N = 2$ (column I), $N = 4$ (column II), and $N = 5$ (column III). Note that additional parameters and initial values of Figs. 14, 15, 16, 17, 18, 19, 20, 21 and 22 are taken from Fig. 13 (color figure online)

cooperators gather in solid circles in the form of speckles, while others disperse in other areas. Column II of Fig. 13 reflects a three-player game with the same parameters. In this case, the solid circle dissipates, and the short streak form of the cooperator increases. Further increasing the density of participants in the game, the cooperators are still mixed patterns of short stripes and spots, the difference being that the density of cooperators increases after the shift from the second column of Fig. 13 to the second column of Fig. 14. When the density of participants playing the game in the unit area increases again, the cooperators form a maze pattern through the long stripe as shown in the third column of Fig. 14. Thus, increasing the density of participants in the game favors cooperators and public goods density, causing cooperators to get closer together and form a long stripe pattern.

5.3 Pattern Formation Due to Spatial Diffusion

Diffusion disrupts the homogeneous distribution of cooperators and public goods in space and induces Turing patterns, manifested in aggregating cooperators and public goods into spots and stripes showing heterogeneous density spatial distribution. We next investigate the influence of diffusion coefficients d_u and d_m on the Turing patterns. The different diffusion coefficients of cooperators create fascinating spatial distributions. If the conditions $b_0 > b_0^*$, $\varepsilon > \varepsilon^*$, and $\frac{d_m}{d_u} > \phi_1$ in Theorem 4.2 are satisfied, the Turing patterns appear as shown in Fig. 15. In Fig. 15a, the cooperators spontaneously gather in the thick stripes. As d_u changes, the coarse stripes are reduced and supplanted by fine stripes and spots. Further increasing the value of d_u, we obtained Fig. 15c, containing circles and rectangles. On this occasion, the distance

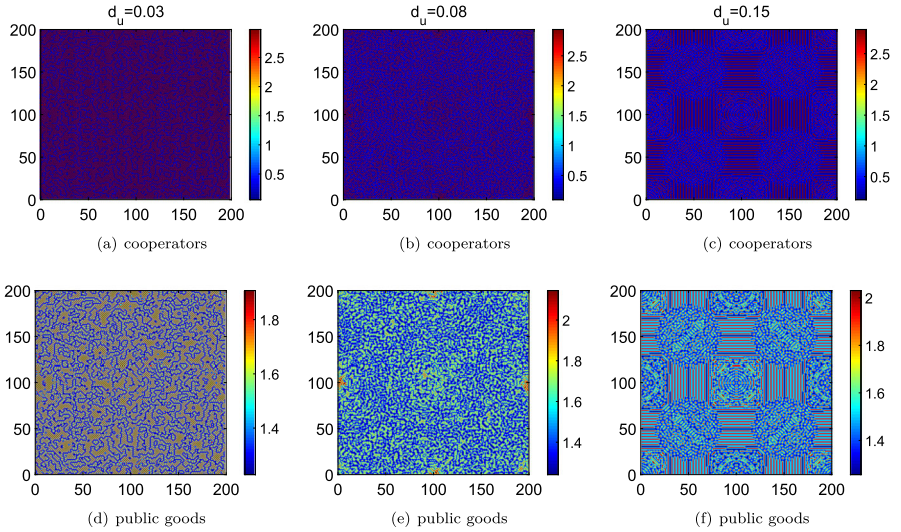

Fig. 15 Spatial distribution of cooperators and public goods with $d_u = 0.03$ (column I), $d_u = 0.08$ (column II), and $d_u = 0.15$ (column III). The value of d_m is 3 (color figure online)

between the cooperators is further increased, the stripes are further thinned, and the spatial domain occupied by the spots becomes wider. Thus, increasing d_u makes the density of cooperators lower. The growing thinness of the stripes and the decentralization of the cooperators increases the chances of contact between cooperators and defectors, which allows defectors to deceive cooperators more easily. Therefore, the stronger the proliferation ability of cooperators, the weaker the cohesion of cooperators, which suppresses players' enthusiasm to choose strategy C and increases the risk of cooperators' extinction. Moreover, public goods gradually decrease, and the harsh survival environment further exacerbates the players' hesitancy to choose cooperative strategies.

The spatial diffusion of public goods stimulates multiple patterns of populations and has a distinguishing impact on the sustainability of cooperation. If inequality $\frac{d_m}{d_u} > \phi_1$ in Theorem 4.2 holds, the Turing instability appears as shown in Fig. 16. Figure 16 considers the impact of the diffusion rate d_m of public goods on the spatial distribution of cooperators and public goods through the Turing pattern. In Fig. 16a, cooperators are loosely distributed and not sufficiently cohesive. Cooperators prefer coarse striped morphological distribution as the diffusion coefficient of public goods rises, as shown in Fig. 16b. The further increasing in diffusion rate of public goods allows for an increased density and cohesiveness of cooperators as shown in Fig. 16c. Therefore, the increase in the diffusion rate of public goods assists players in adopting cooperative strategies. Interestingly, the distribution of public goods and cooperators form a similar overall profile except for the different intensities. Adequate public goods attract cooperators, who produce public goods, which further increases the level of public goods density, and then a suitable living environment is conducive to the reproduction of cooperators. Public goods and cooperators promote each other for

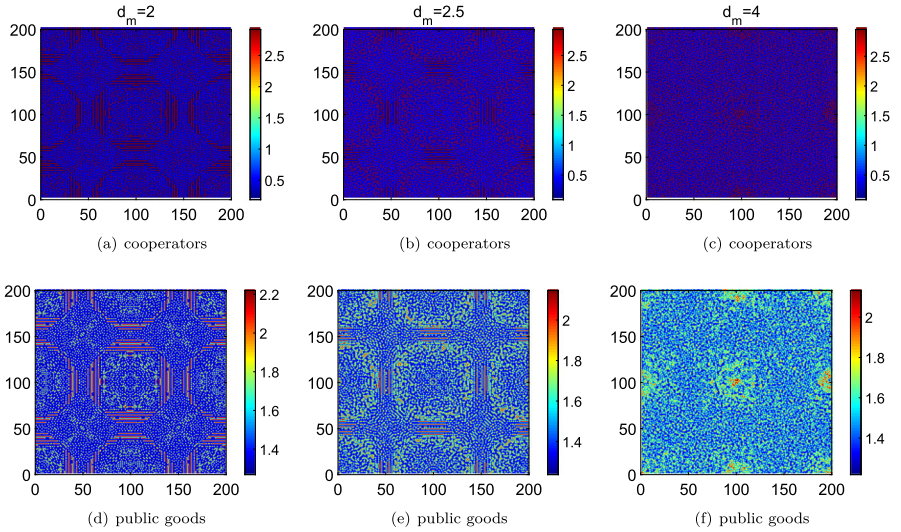

Fig. 16 Spatial distribution of cooperators and public goods with $d_m = 2$ (column I), $d_m = 2.5$ (column II), and $d_m = 4$ (column III). The value of d_u is 0.1 (color figure online)

mutual benefit. The diffusion rates of public goods and cooperators affect not only the development of patterns but also the strategies employed by the players, thus affecting the sustainability of the population.

5.4 Pattern Formation and Chaos Due to Payoffs

Figures 17 and 20 depict the effects of payoffs a_0 and a_1 on the spatio-temporal dynamics of the cooperators, respectively. They reveal chaotic spatial patterns of cooperators, mainly reflected in changing and chaotic spatial distributions over time and parameters. Interestingly, the cooperators exhibit a regular centrosymmetric and axisymmetric distribution in the early stages of evolution, which can be seen in the first two rows of Figs. 17 and 20. Mixed distributions of chaotic patterns occur in the later stages of evolution (the last two rows of Figs. 17 and 20). The tendency towards chaos is almost unaffected by the changes in parameter values, with two exceptions. An intermediate value of a_1 results in earlier chaos formation, whereas a large value of a_1 leads to defectors' extinction, resulting in no chaotic patterns. Stationary patterns emerge in the second column of Fig. 13, and the distribution of cooperative behavior in space remains unchanged after some time. Increasing the value of a_0 yields Fig. 17, which shows the chaotic patterns. The transition from the second column of Figs. 13, 14, 15, 16 and 17 suggests that the increase in a_0 causes uncertainty in the evolutionary outcome of the cooperators. In general, an increase in a_0 benefits cooperators after a certain time of evolution by encouraging them to gather together and increasing the chances of survival of cooperative clusters. The same, but more pronounced effect is observed due to an increase in a_1. Thus, the evolutionary outcomes of strategies and public goods are more sensitive to players' payoffs under abundant public goods conditions than

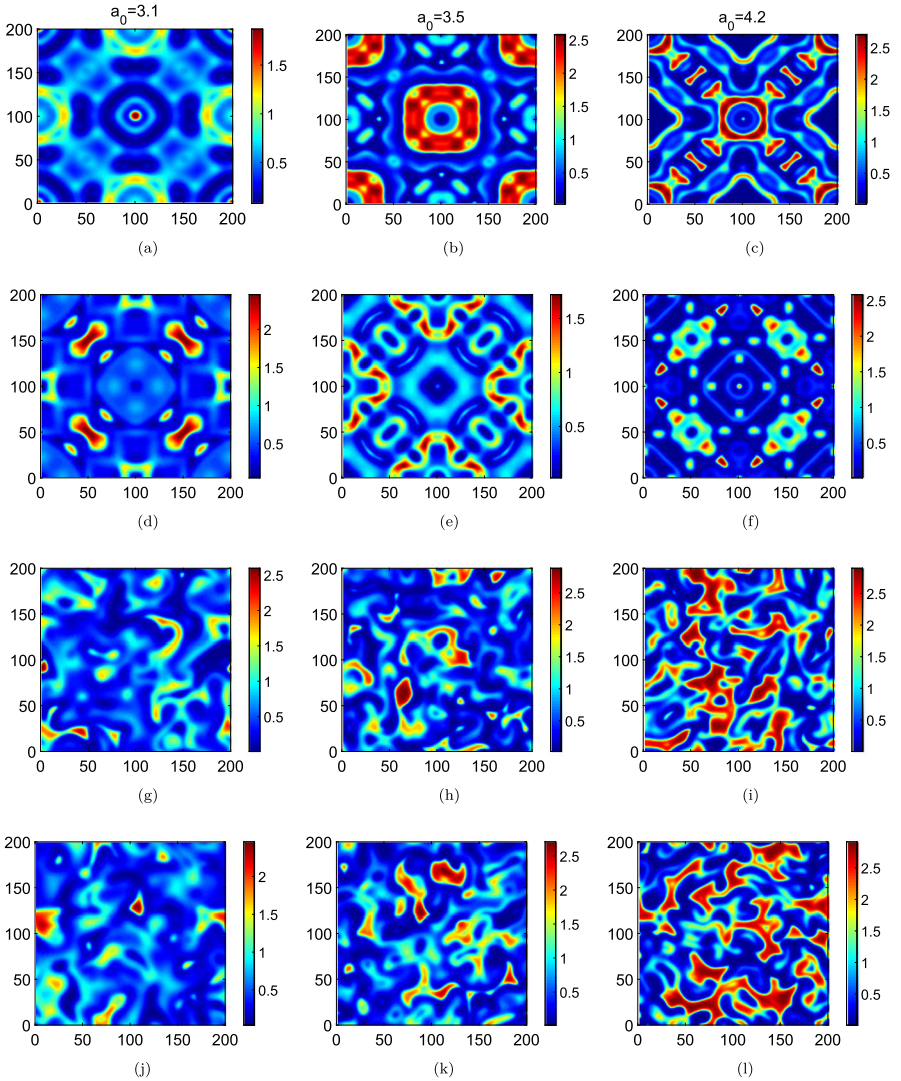

Fig. 17 Spatial distribution of cooperators at times $t = 500$ (row I), $t = 1000$ (row II), $t = 10000$ (row III), and $t = 50000$ (row IV) with $a_0 = 3.1$ (column I), $a_0 = 3.5$ (column II), and $a_0 = 4.2$ (column III) (color figure online)

under scarce conditions. For the diffusion system (2.4), it is intriguing that a_0 takes values from the stable interval of the non-diffusion system (2.3). However, unlike the non-diffusion system, the diffusion system exhibits heterogeneous distributions containing stationary and chaotic patterns, as shown in Fig. 17 and column II of Fig. 13. Therefore, comparing the diffusion system with the non-diffusion system, diffusion coefficients induce stationary and chaotic patterns for the cooperators.

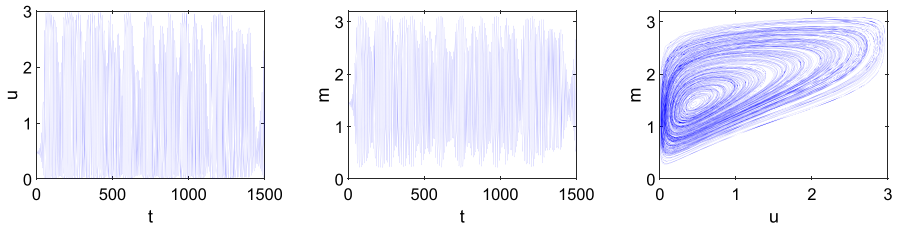

(a) cooperators (b) public goods (c) phase portrait in $u - m$ plane

Fig. 18 The chaotic behavior occurs at position (100,100) with $a_0 = 3.1$ (color figure online)

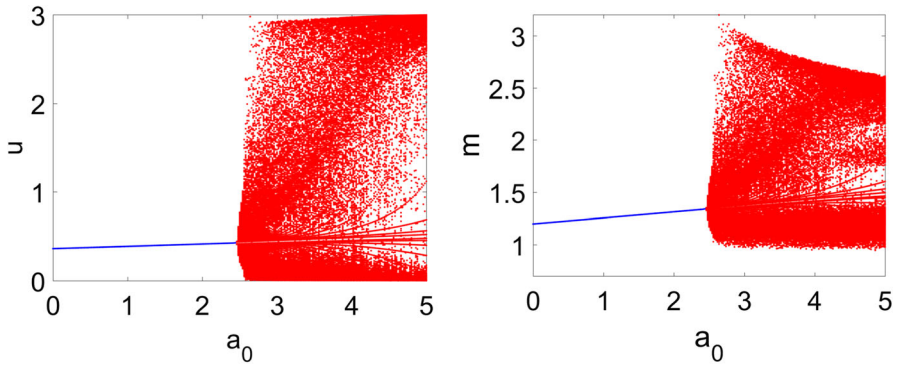

(a) cooperators (b) public goods

Fig. 19 The chaos induced by a_0 at position (100,100). The blue part indicates that system (2.4) is spatially stable. The red part indicates that chaos appears in system (2.4) (color figure online)

To show the appearance of chaotic behavior in system (2.4) due to a_0 we plot Fig. 18. In Fig. 18a and b, the cooperators and public goods evolve over time with irregular oscillations, which manifest the emergence of chaos. Notice that the value of cooperators is equal to zero in some cases, which means that cooperators sometimes go extinct, but not all the time. The value of the public goods is always greater than zero, demonstrating that the public goods supply is never interrupted in the population. In Fig. 18c, the phase trajectory eventually does not stabilize at a point or limit cycle but keeps evolving haphazardly, reflecting chaos. Cooperators and public goods transform from spatial stability to chaos as a_0 changes as shown in Fig. 19. When the value of a_0 is taken from the interval corresponding to the blue part in Fig. 19, system (2.4) is spatially stable at E_-^*. Under this scenario, the density of cooperators and public goods concentration increase with a_0, suggesting that increasing the value of a_0 assists the cooperators, similar to the role of a_0 in the non-diffusion system (2.3) shown in Fig. 5b. Unlike the non-diffusion system, the diffusion system develops fascinating chaotic dynamics when a_0 exceeds a certain threshold. The parameter values in Figs. 17 and 18 are chosen from the red chaotic interval of Fig. 19. Under these circumstances, both cooperators and defectors have the opportunity to dominate parts of the area, and public goods remain in supply.

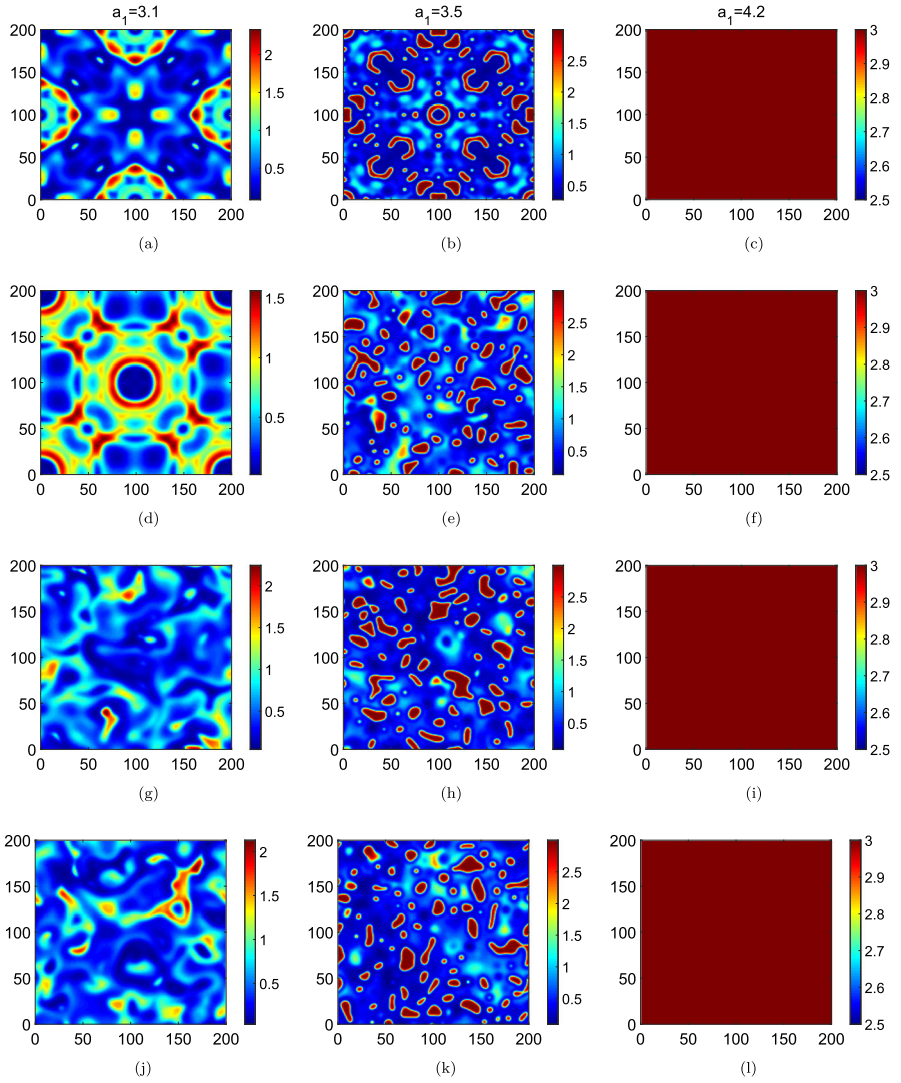

Fig. 20 Spatial distribution of cooperators at times $t = 500$ (row I), $t = 1000$ (row II), $t = 10{,}000$ (row III), and $t = 50{,}000$ (row IV) with $a_1 = 3.1$ (column I), $a_1 = 3.5$ (column II), and $a_1 = 4.2$ (column III) (color figure online)

The coexistence of the chaotic and homogeneous patterns captures the effect of the payoff a_1 on the spatial distribution of cooperators when they meet in high-density public goods. The location where the spots and hills are located is favored by the cooperators in Fig. 20a. The spots and hills disappear, and the hollow forked symbol pattern appears in the middle of evolution. The first two subplots in the first column are centrosymmetric and axially symmetric, which explains the regularity of the distribution of cooperators during their early evolution. After a period of evolution, the

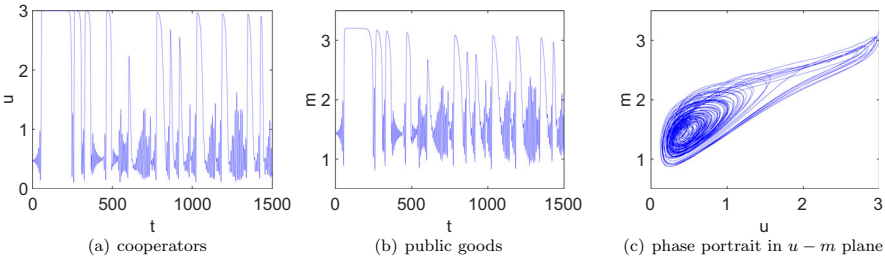

Fig. 21 The chaotic behavior occurs at position (100, 100) with $a_1 = 3.5$ (color figure online)

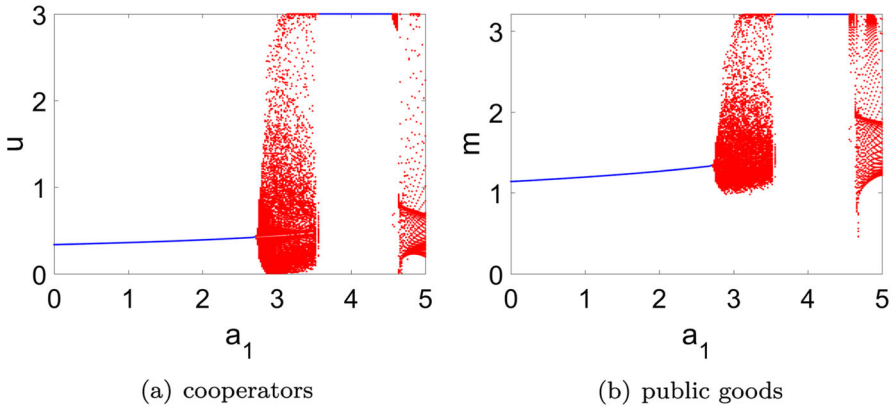

Fig. 22 The chaos induced by a_1 at position (100, 100). The blue part indicates that system (2.4) is spatially stable. The red part indicates that chaos appears in system (2.4) (color figure online)

spatial distribution of cooperators shows irregular mixed patterns of stripes and spots in Fig. 20g and j. The second column is obtained by increasing the value of a_1 in the first column. Unsurprisingly, the maximum level of cooperator density increases with an increase of a_1. Surprisingly, the symmetrical pattern does not appear but rather a chaotic pattern in mid-evolution, demonstrating that the increase in a_1 leads to an accelerated cooperative irregularity. Further increasing in a_1 leads cooperators to evolve from a heterogeneous initial state to homogeneity. In this case, the density of defectors is zero, and cooperators occupy the entire population. When a_1 is relatively small, the cooperators and defectors end up with a statically heterogeneous distribution in space, as shown in column II of Fig. 13. Under the circumstances, small a_1 brings stable heterogeneous distributions. Moderate a_1 leads to chaotic patterns, which exposes cooperators to uncertain environments and challenges cooperative behavior. Further increasing a_1 allows only cooperative behavior in the population, in which it is in the best interest for cooperators to be protected from the risk of being cheated by defectors.

The time series of cooperators and public goods in Fig. 21 exhibit disorderly oscillations, reflecting the chaotic dynamics that happen in system (2.4). The erratic advance of the phase trajectory indicates the presence of chaos. Figure 22 presents the inter-

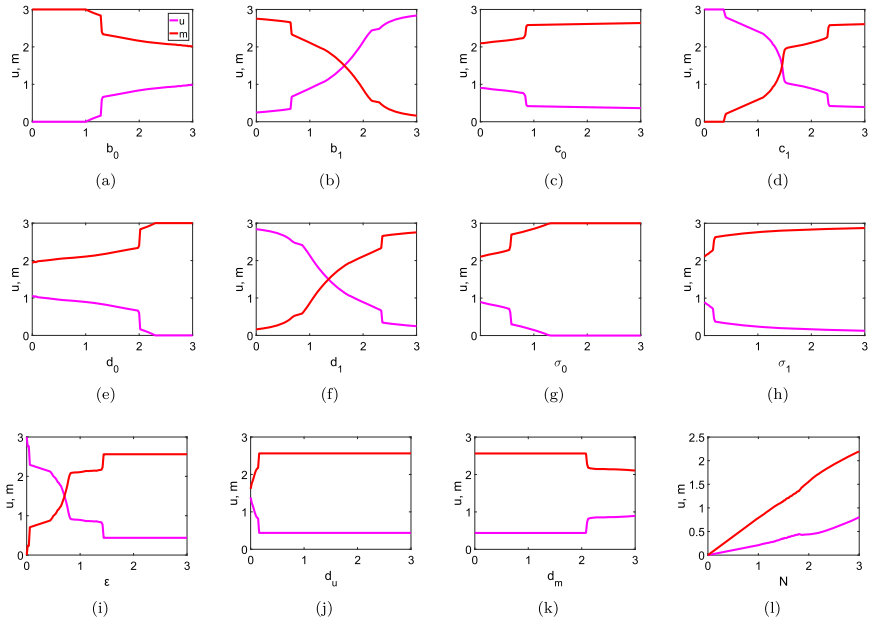

Fig. 23 Dependence of cooperators' and public goods' densities in system (2.4) on different parameters. The magenta and red curves indicate the spatially averaged density of cooperators and public goods, respectively (color figure online)

conversion of system (2.4) between spatially stable and chaotic states due to a_1. The blue and red parts correspond to spatial stability and spatial-temporal chaos states, respectively. System (2.4) is spatially stable at E^*_- when a_1 corresponds to the first blue interval. Increasing the value of a_1 within this interval promotes the prosperity of cooperators. When a_1 exceeds the upper limit of the interval, the diffusion system changes from spatial stability to chaos, which is consistent with the phenomena depicted in Figs. 20 and 21. In this case, the values of the cooperators transform irregularly between zero and N, which allows the pure cooperators to occupy certain regions. The system turns spatially stable when a_1 corresponds to the second blue interval, in which case defectors become extinct, and cooperators occupy the entire population. Once a_1 reaches the red part again, the diffusion system (2.4) switches from spatial stability to chaos. Regardless of whether the diffusion system is spatially stable or chaotic, the density of public goods is always greater than zero, and therefore public goods are continuously supplied.

We restrict the parameters to the same range and explore their sensitivity by examining how the average density of the spatial distribution for cooperators and public goods changes with these parameters (see Fig. 23). Changing the values of the parameters does not affect the spatially averaged density of the cooperators when $b_0 \in (0, 1)$, $\sigma_0 \in (1.32, 3)$, $\varepsilon \in (1.44, 3)$, $d_u \in (0.17, 3)$, and $d_m \in (0, 2.08)$. We observe that increasing the benefit of cooperators, the diffusion rate of public goods, and player density favor cooperation. In addition, decreasing the benefit of defectors, the cost

of cooperation, the relative timescale, and the diffusion rate of cooperators can promote cooperation. The evolutionary outcome of the cooperators is sensitive to the parameters b_1, c_1, d_1 and ε.

6 Discussion

Eco-evolutionary game systems that involve mutual feedback between strategy and environment frequently arise across different spheres of life. In ecology, one can consider a model with two strategies, each of which leads to producing the pollutant as a byproduct at different rates. Here the pollutant might be considered as a decaying resource, affecting the environment (Tilman et al. 2020). In psychology, deliberative and thoughtful decision-making can design an advantageously shared environment of social norms and institutions, but in this new environment less costly, non-deliberative decision-making benefits, forming cognition-environment feedback (Rand et al. 2017). In biology, there is mutual feedback between strategies and public goods. In microbial cooperation, public goods such as siderophores, enzymes, and biosurfactants (Smith and Schuster 2019) produced by cooperators in microbial populations impact the environment in which microbial populations live. Players in the microbial population choosing cooperative strategies influence the density of public goods. The density of public goods in turn affects the fitness of the strategies chosen by individuals in the microbial population. Siderophores produced by cooperators help *Pseudomonas aeruginosa* to scavenge iron in iron-depleted environments during quorum sensing (Diggle et al. 2007). Defectors utilize siderophores by deception.

However, research on eco-evolutionary game systems with spatial diffusion remains scarce. We aim to investigate cooperative strategy and public goods dynamics in the eco-evolutionary game with environmental feedback under well-mixed and heterogeneous environmental conditions. The focus of this work is on linear two-strategy eco-evolutionary games in which actors can adopt one of two strategies—a cooperative strategy to extract the resources at a cost and a defective strategy only to consume the same resource. Even this most straightforward form of evolutionary game enables substantial analysis of the spatio-temporal evolutionary patterns of cooperation and public goods distribution. Such kind of interaction can be demonstrated through experimental competitions between isogenic respirer (cooperator) and respiro-fermenter (cheater) yeast strains with alternative pathways of glucose metabolism (MacLean and Gudelj 2006). There is a significant difference between competition in a homogeneous environment (glucose-limited chemostats) and in a spatially structured environment (glucose-limited batch cultures), where competition results in the extinction of the cooperators and stable coexistence of both yeast strains, respectively.

In this study, we propose two models. Our first model combines replicator and public goods dynamics under well-mixed environment conditions (2.3), and the second model is a heterogeneous model with spatial diffusion (2.4). In our models, the fitness of cooperative and defecting strategies depends on two payoff matrices corresponding to poor or abundant public goods conditions, current public goods concentration, and δ. In the resulting systems, we account for such parameters as player density, relative timescale, maximum productivity, the saturation parameter of production, and public

goods consumption rate. As shown in Figs. 1, 2, 3, 4, 5, 6 and 7 for temporal system and in Figs. 8, 9, 10, 11, 12, 13, 14, 15, 16, 17, 18, 19, 20, 21 and 22 for diffusion system, each of those parameters can have a strong effect on the game dynamics. Unlike the multiscale analysis (Heggerud et al. 2020), we find that relative timescales can lead to Hopf bifurcations in both mixed and heterogeneous environments. In this study, we analyze the influence of each parameter and some pairs of parameters on the evolution of the system with fixed values of the remaining parameters, based on previous works (Weitz et al. 2016; Tilman et al. 2020; Cheng et al. 2023). We also explore various dynamical properties of the obtained systems, including the existence and local stability of equilibria, bistability, transcritical, and Hopf bifurcations in the temporal system, and spatial stability, Turing instability, Hopf and Turing–Hopf bifurcations, Turing patterns formation in the diffusion system. Hence, we provide a mathematical approach and theoretical framework for exploring the spatio-temporal dynamics of eco-evolutionary game systems from an ordinary and partial differential perspective.

The presence and stability of equilibria reveal diverse evolutionary outcomes of cooperators and public goods, shedding light on the effectiveness of strategies and the adequacy of public goods. Some previous experimental studies have focused on identifying the factors that can benefit cooperators. It was shown that a higher initial population density in batch cultures leads to a higher equilibrium frequency of yeast cooperative strain (MacLean and Gudelj 2006). Using iron-scavenging siderophore pyoverdine as a model public goods for the bacterium *Pseudomonas aeruginosa* in different environments, it was observed that the most potent beneficial factor for cooperators was the reduction of individual dispersal (Figueiredo et al. 2021). In our investigation of the temporal and diffusion models, we found several factors that positively influence cooperator density. Such factors turn to be the player density (Figs. 4f, 7q–t, 14), decreasing the relative timescale (Figs. 4d, 5a, 12, 13), improving the diffusion rate of the public goods (Fig. 16), and lowering the diffusion rate of the cooperators (Fig. 15). However, for such multi-parameter systems, it is vital to consider a combination of all the factors when predicting the impact on cooperation and public goods dynamics. Typically, when more individuals work together towards a common goal, the benefits that come from that shared effort are greater. Yet, it is crucial to take all system parameters into account when examining the impact on the cooperation and availability of public goods. Our model suggests that a greater density of cooperators doesn't necessarily result in greater public goods density. Specifically, if the δ is significant, increasing players' density benefits cooperators, simultaneously making the public goods more barren (Fig. 7q–t). Also, if the consumption rate of resources is large, cooperators dominate, but public goods remain scarce (Fig. 7m–p).

Studying the combined effects of payoffs taken from poverty and richness payoff matrices, also provides some counterintuitive conclusions. Increasing the cooperator's payoff while encountering defectors should increase the cooperator's likelihood of survival. However, as shown in Fig. 7e–h, this trend might change at certain parameter values. Similarly, increasing the defector's payoff should improve their chances of survival, but under certain conditions, raising the defector–defector payoff in a poor public goods environment could benefit cooperators (Fig. 7k–l). In a diffusion system, increasing already large cooperator–cooperator payoff under abundant public goods conditions leads to a shift from the chaotic coexistence of cooperators and defectors

to the dominance of cooperators. However, with a further increase of that payoff, the chaotic pattern returns (Fig. 22). Moreover, the system's bistability makes it crucial to consider not just the parameters but also the initial state of the system for correct predictions of its behavior. Figure 3 illustrates how the system's various initial states can result in different evolutionary outcomes, ranging from cooperators' dominance to the coexistence of both strategies, or to the defectors' dominance. Therefore, it is essential to consider all factors and the initial state of the system combined in order to obtain accurate results.

To make the analysis of such systems easier, we present theorems for both non-diffusion and spatial diffusion models in this paper. These theorems provide conditions for the existence and stability of equilibria, and the occurrence of transcritical, Hopf, and Turing–Hopf bifurcations. Thus, we obtain a mathematical framework for studying the spatio-temporal dynamics of eco-evolutionary game systems with environmental feedback under well-mixed and heterogeneous environmental conditions. This theoretical framework will help to accurately predict the dynamics of cooperation and public goods distribution for ecological and biological systems where actors extract growth-limiting resources from their surroundings. However, certain aspects require further investigation. For instance, it would be of practical significance to investigate time delays (Xu et al. 2018; Yuan and Meng 2022; Wang and Cheng 2016) and environmental fluctuations (Zhao et al. 2022) in evolutionary game systems with spatial diffusion. Additionally, considering spatial diffusion within the context of multi-strategy games (Duong and Han 2016a, b) or multi-games (Cheng and Meng 2023; Chowdhury et al. 2021b) would also be worth further study.

A Proof of Theorem 3.1

Proof (I) The Jacobian matrix for $E_1(0, 0)$ is

$$J_1 = \begin{pmatrix} \delta(b_0 - d_0) & 0 \\ \frac{\beta\varepsilon}{\alpha} & -Nk\varepsilon \end{pmatrix}.$$

The eigenvalues of J_1 are $\delta(b_0 - d_0)$ and $-Nk\varepsilon < 0$. E_1 is stable when $d_0 > b_0$. On the contrary, E_1 is a saddle point when $d_0 < b_0$.
(II) The Jacobian matrix at $E_2(N, \frac{\beta}{k(\alpha+N)})$ is calculated as

$$J_2 = \begin{pmatrix} \delta(c_0 - a_0) - \frac{\beta(\eta_1+\eta_2)}{k(N+\alpha)} & 0 \\ \frac{\beta\alpha\varepsilon}{(N+\alpha)^2} & -Nk\varepsilon \end{pmatrix}.$$

The eigenvalues are $\delta(c_0 - a_0) - \frac{\beta(\eta_1+\eta_2)}{k(N+\alpha)}$ and $-Nk\varepsilon < 0$. The sign of $\delta(c_0 - a_0) - \frac{\beta(\eta_1+\eta_2)}{k(N+\alpha)}$ governs the stability of E_2. E_2 is stable if $\delta(c_0 - a_0) < \frac{\beta(\eta_1+\eta_2)}{k(N+\alpha)}$. E_2 is a saddle point when $\delta(c_0 - a_0) > \frac{\beta(\eta_1+\eta_2)}{k(N+\alpha)}$.

(III) The Jacobian matrix corresponding to the positive equilibrium $E_-^*(u_-^*, m_-^*)$ is given by

$$J^* = \begin{pmatrix} j_{11}^* & j_{12}^* \\ j_{21}^* & j_{22}^* \end{pmatrix},$$

where

$$j_{11}^* = \frac{u_-^*}{N^2}\left[((\eta_1 - \eta_2)N - 2\eta_1 u_-^*)m_-^* + \delta((d_0 - b_0 - \eta_3)N + 2\eta_3 u_-^*)\right],$$
$$j_{12}^* = \frac{u_-^*(N - u^*)}{N^2}(\eta_1 u_-^* - N\eta_2), \quad j_{21}^* = \frac{\alpha\beta\varepsilon}{(u_-^* + \alpha)^2}, \quad j_{22}^* = -Nk\varepsilon.$$

The characteristic equation is

$$\lambda^2 - \mathrm{tr}(J^*)\lambda + \det(J^*) = 0, \tag{A.1}$$

where $\mathrm{tr}(J^*) = j_{11}^* + j_{22}^*$ and $\det(J^*) = j_{11}^* j_{22}^* - j_{21}^* j_{12}^*$. The stability of $E_-^*(u_-^*, m_-^*)$ is determined by the signs of $\mathrm{tr}(J^*)$ and $\det(J^*)$. Some calculations reveal that $\mathrm{tr}(J^*) < 0$ (resp. $\mathrm{tr}(J^*) > 0$) and $\det(J^*) > 0$ (resp. $\det(J^*) < 0$) when $\varepsilon > \varepsilon^*$ (resp. $\varepsilon < \varepsilon^*$) and $b_0 > b_0^*$ (resp. $b_0 < b_0^*$). Therefore, $E_-^*(u^*, m^*)$ is stable if $\varepsilon > \varepsilon^*$ and $b_0 > b_0^*$. If $\varepsilon < \varepsilon^*$ and $b_0 > b_0^*$, then $E_-^*(u_-^*, m_-^*)$ is an unstable node or focus. In other cases, $E_-^*(u_-^*, m_-^*)$ is a saddle point.
(IV) Note that the analytical procedure for the stability of equilibrium $E_+^*(u_+^*, m_+^*)$ is similar to that for $E_-^*(u_-^*, m_-^*)$. We will not go into details here. This completes the proof. □

B Proof of Theorem 3.2 and Values of the Parameters

Proof The two expressions on the right-hand side of (2.3) are denoted K_1 and K_2, respectively.
(I) d_0 is selected as the bifurcation parameter. When $d_0 = b_0$, the eigenvalues regarding J_1 are zero and $-k\varepsilon N < 0$. The eigenvectors of J_1 and J_1^T concerning zero are

$$L_1 = \begin{pmatrix} 1 \\ \frac{\beta}{Nk\alpha} \end{pmatrix}, \quad M_1 = \begin{pmatrix} 1 \\ 0 \end{pmatrix}.$$

Then, we have

$$K_{d_0}(E_1; b_0) = \begin{pmatrix} \frac{u}{N^2}(N-u)^2(m-\delta) \\ 0 \end{pmatrix}_{(E_1; b_0)} = \begin{pmatrix} 0 \\ 0 \end{pmatrix},$$
$$DK_{d_0}(E_1; b_0)L_1 = \begin{pmatrix} \frac{3u^2+N^2-4uN}{N^2} & \frac{u(u^2+N^2-2uN)}{N^2} \\ 0 & 0 \end{pmatrix} \begin{pmatrix} 1 \\ \frac{\beta}{Nk\alpha} \end{pmatrix}_{(E_1; b_0)} = \begin{pmatrix} 1 \\ 0 \end{pmatrix},$$

$$D^2K(E_1;b_0)(L_1,L_1)=\begin{pmatrix}K_{1uu}+\frac{2\beta}{Nk\alpha}K_{1um}+\frac{\beta^2}{(Nk\alpha)^2}K_{1mm}\\ K_{2uu}+\frac{2\beta}{Nk\alpha}K_{2um}+\frac{\beta^2}{(Nk\alpha)^2}K_{2mm}\end{pmatrix}_{(E_1;b_0)}$$
$$=\begin{pmatrix}\frac{2}{N^2k\alpha}(\delta k\alpha(3-N)(c_0-a_0)+\beta N(b_1-d_1))\\ -\frac{2\varepsilon\beta}{\alpha^2}\end{pmatrix},$$

where

$$K_{1uu}=\frac{1}{N^2}[-6\eta_1um+6\delta\eta_3-2N(2\eta_2-\eta_1-\eta_2)m+2N\delta(d_0-b_0-\eta_3)],$$
$$K_{1um}=\frac{1}{N^2}[-3\eta_1u^2+2N(2\eta_2-\eta_1-\eta_2)u+N^2\eta_2],$$
$$K_{1mm}=0,\quad K_{2uu}=\frac{-2\varepsilon\beta\alpha}{(\alpha+u)^3},\quad K_{2um}=K_{2mm}=0.$$

Thus,

$$M_1^TK_{d_0}(E_1;b_0)=0,$$
$$M_1^TDK_{d_0}(E_1;b_0)L_1=1\neq 0,$$
$$M_1^TD^2K(E_1;b_0)(L_1,L_1)=\frac{2}{N^2k\alpha}(\delta k\alpha(3-N)(c_0-a_0)+\beta N(b_1-d_1))\neq 0.$$

So we conclude that when $d_0=b_0$, there is a transcritical bifurcation at $E_1(0,0)$.
(II) For J_2, the eigenvalues are $-Nk\varepsilon$ and zero when $\delta=\delta^*=\frac{\beta(a_0-a_1-c_0+c_1)}{(a_0-c_0)(N+\alpha)k}$. For the eigenvalue zero, the eigenvectors of J_2 and J_2^T are given by

$$L_2=\begin{pmatrix}1\\ \frac{\beta\alpha}{Nk(N+\alpha)^2}\end{pmatrix},\quad M_2=\begin{pmatrix}1\\0\end{pmatrix}.$$

Further,

$$K_\delta(E_2;\delta^*)=\begin{pmatrix}\frac{u(N-u)}{N^2}(-\eta_3u-N(d_0-b_0))\\ 0\end{pmatrix}_{(E_2;\delta^*)}=\begin{pmatrix}0\\0\end{pmatrix},$$
$$DK_\delta(E_2;\delta^*)L_2=\begin{pmatrix}\gamma_4&0\\0&0\end{pmatrix}\begin{pmatrix}1\\ \frac{\beta\alpha}{Nk(N+\alpha)^2}\end{pmatrix}_{(E_2;\delta^*)}=\begin{pmatrix}c_0-a_0\\0\end{pmatrix},$$
$$D^2K(E_2;\delta^*)(L_2,L_2)=\begin{pmatrix}K_{1uu}+\frac{2\beta\alpha}{Nk(N+\alpha)^2}K_{1um}+\frac{(\beta\alpha)^2}{(Nk)^2(N+\alpha)^4}K_{1mm}\\ K_{2uu}+\frac{2\beta\alpha}{Nk(N+\alpha)^2}K_{2um}+\frac{(\beta\alpha)^2}{(Nk)^2(N+\alpha)^4}K_{2mm}\end{pmatrix}_{(E_2;\delta^*)}$$
$$=\begin{pmatrix}\gamma_5\\ -\frac{2\varepsilon\beta\alpha}{(\alpha+N)^3}\end{pmatrix},$$

Table 3 The values of the parameters

	a_0	a_1	b_0	b_1	c_0	c_1	d_0	d_1	σ_0	σ_1	δ	β	α	k	N	ε
(1)	2.9	4	0	1	0.1	2	1	2	0.02	0.01	2	2.5	0.9	0.2	3	1
(2)	2.9	3	2.3	1	0.1	2	1	2	0.02	0.01	2	2.5	0.9	0.2	3	1
(3)	2	3	2	5	1	6	5	2	0.02	0.01	7	5	0.9	0.2	2	1
(4)	2.1	3	2.1	1	0.1	2	2.2	2	0.02	0.01	2	2.5	0.9	0.2	3	1

The parameters of Figs. 1a–c, and 2a, b are taken from (1), (2), (3), and (4), respectively. The parameters of Fig. 3a and b are chosen from (4) and (3), respectively. The parameters in the remaining figures are taken from (2)

where

$$\gamma_4 = \frac{1}{N^2}(3\eta_3 u^2 + 2N(d_0 - b_0 - \eta_3)u - N^2(d_0 - b_0)),$$
$$\gamma_5 = \frac{2\beta}{kN(\alpha+N)}(-2\eta_1 - \eta_2) + \frac{-2\beta(\eta_1+\eta_2)}{(a_0-c_0)(N+\alpha)kN^2}(3\eta_3 + N(d_0 - b_0 - \eta_3)) + \frac{2\beta\alpha}{N^3k(N+\alpha)^2}(-7(\eta_1+\eta_2) + 8\eta_2).$$

Therefore,

$$M_2^T K_\delta(E_2; \delta^*) = 0,$$
$$M_2^T DK_\delta(E_2; \delta^*)L_2 = c_0 - a_0 \neq 0,$$
$$M_2^T D^2K(E_2; \delta^*)(L_2, L_2) = \gamma_5 \neq 0.$$

Consequently, a transcritical bifurcation appears at $E_2(N, \frac{\beta}{k(\alpha+N)})$ when $\delta = \delta^*$.
(III) We know that $\mathrm{tr}(J^*) = 0$ and $\det(J^*) > 0$ if $\varepsilon = \varepsilon^*$ and $b_0 > b_0^*$. When $\varepsilon = \varepsilon^*$, $\lambda_{11} = i\sqrt{\det(J^*)}$ and $\lambda_{12} = -i\sqrt{\det(J^*)}$ are the pure imaginary roots of (A.1). From (A.1), we deduce that

$$\left[\frac{d\mathrm{Re}\lambda}{d\varepsilon}\right]_{\lambda=\lambda_{11},\,\varepsilon=\varepsilon^*} = \frac{1}{2}\left[\frac{d(\mathrm{tr}(J^*)}{d\varepsilon}\right]_{\varepsilon=\varepsilon^*} = -\frac{Nk}{2} < 0.$$

Thus, a Hopf bifurcation emerges near $E_-^*(u_-^*, m_-^*)$ if $\varepsilon = \varepsilon^*$ and $b_0 > b_0^*$. This completes the proof. □

C Proof of Theorem 3.3

Proof Let $\hat{u} = u - u^*$ and $\hat{m} = m - m^*$. For convenience, $\hat{u}$ and $\hat{m}$ are still denoted by u and m, respectively. Then system (2.3) is rewritten as

$$\begin{cases} \frac{du}{dt} = \frac{(u+u^*)}{N^2}(N-u-u^*)[(\eta_1(u+u^*)+N\eta_2)(m+m^*) \\ \quad -\delta(\eta_3(u+u^*)+N(d_0-b_0))], \\ \frac{dm}{dt} = \varepsilon\left(\frac{\beta(u+u^*)}{\alpha+u+u^*} - kN(m+m^*)\right). \end{cases} \tag{C.1}$$

Applying the Taylor expansion, system (C.1) becomes

$$\begin{pmatrix} u_t \\ m_t \end{pmatrix} = J^* \begin{pmatrix} u \\ m \end{pmatrix} + \begin{pmatrix} g(u,m,\varepsilon) \\ h(u,m,\varepsilon) \end{pmatrix}. \tag{C.2}$$

For the nonlinear terms $g(u, m, \varepsilon)$ and $h(u, m, \varepsilon)$ are given by

$$\begin{aligned} g(u,m,\varepsilon) &= g_1u^2 + g_2um + g_3u^3 + g_4u^2m + \cdots, \\ h(u,m,\varepsilon) &= h_1u^2 + h_2u^3 + \cdots, \end{aligned}$$

where

$$\begin{aligned} g_1 &= \frac{1}{N^2}\left(3\delta\eta_3u^* - N(\eta_2-\eta_1)u^*m^* - 3\eta_1u^*m^* + N\delta(d_0-b_0-\eta_3)\right), \\ g_2 &= \frac{1}{N^2}(N^2\eta_2 - 3\eta_1u^{*2} - 2N(\eta_2-\eta_1)u^*), \\ g_3 &= \frac{1}{N^2}(\delta\eta_3 - \eta_1m^*), \quad g_4 = \frac{1}{N^2}(N(\eta_1-\eta_2) - 3\eta_1u^*), \\ h_1 &= -\frac{\varepsilon\beta}{(\alpha+u^*)^3}, \quad h_2 = \frac{\varepsilon\beta}{(\alpha+u^*)^4}. \end{aligned}$$

The characteristic roots of J^* are denoted as $\lambda_{13} = \varphi + i\rho$ and $\lambda_{14} = \varphi - i\rho$, where $\varphi = \frac{\mathrm{tr}(J^*)}{2}$ and $\rho = \sqrt{\det(J^*) - \left(\frac{\mathrm{tr}(J^*)}{2}\right)^2}$. When $4\det(J^*) > \mathrm{tr}^2(J^*)$, λ_{13} and λ_{14} are conjugate complexes. In particular, $\lambda_{13} = i\rho$ and $\lambda_{14} = -i\rho$ are pure imaginary numbers when $\varepsilon = \varepsilon^*$. Then the eigenvector of J^* about $\lambda_{13} = \varphi + i\rho$ is

$$\theta = \begin{pmatrix} 1 \\ \theta_1 - i\theta_2 \end{pmatrix},$$

where $\theta_1 = \frac{\varphi - j_{11}^*}{j_{12}^*}$ and $\theta_2 = -\frac{\rho}{j_{12}^*}$.

Let

$$\Theta = \begin{pmatrix} 1 & 0 \\ \theta_1 & \theta_2 \end{pmatrix}.$$

By the following conversion,

$$\begin{pmatrix} u \\ m \end{pmatrix} = \Theta \begin{pmatrix} s \\ z \end{pmatrix},$$

system (C.2) yields

$$\begin{pmatrix} \frac{ds}{dt} \\ \frac{dz}{dt} \end{pmatrix} = \begin{pmatrix} \varphi & -\rho \\ \rho & \varphi \end{pmatrix} \begin{pmatrix} s \\ z \end{pmatrix} + \begin{pmatrix} P(s,z) \\ Q(s,z) \end{pmatrix}, \tag{C.3}$$

where

$$\begin{aligned} P(s,z) &= p_1 s^2 + p_2 sz + p_3 s^3 + p_4 s^2 z + \cdots, \\ Q(s,z) &= h_1 s^2 + h_2 s^3 + \cdots, \end{aligned}$$

with

$$p_1 = g_1 + g_2\theta_1, \quad p_2 = g_2\theta_2, \quad p_3 = g_3 + g_4\theta_1, \quad p_4 = g_4\theta_2.$$

We formulate system (C.3) in polar form as follows

$$\begin{cases} \dfrac{dr_0}{dt} = \varphi(\varepsilon) r_0 + S_1(\varepsilon) r_0^3 + \cdots, \\ \dfrac{d\theta_0}{dt} = \rho(\varepsilon) + S_2(\varepsilon) r_0^2 + \cdots. \end{cases} \tag{C.4}$$

If $\varepsilon = \varepsilon^*$, by the Taylor expansion, (C.4) leads to

$$\begin{cases} \dfrac{dr_0}{dt} = \varphi'(\varepsilon^*)(\varepsilon - \varepsilon^*) r_0 + S_1(\varepsilon^*) r_0^3 + \cdots, \\ \dfrac{d\theta_0}{dt} = \rho(\varepsilon^*) + \rho'(\varepsilon^*)(\varepsilon - \varepsilon^*) + S_2(\varepsilon^*) r_0^2 + \cdots. \end{cases}$$

We next explore the positivity and negativity for the coefficient $S_1(\varepsilon^*)$.

$$\begin{aligned} S_1(\varepsilon^*) = \frac{1}{16}[P_{sss} + P_{szz} + Q_{ssz} + Q_{zzz}] + \frac{1}{16\rho(\varepsilon^*)}[P_{sz}(P_{ss} + P_{zz}) \\ - Q_{sz}(Q_{ss} + Q_{zz}) - P_{ss}Q_{ss} + P_{zz}Q_{zz}]|_{(0,0,\varepsilon^*)}, \end{aligned}$$

where

$$\begin{aligned} &P_{sss}(0,0,\varepsilon^*) = 6p_3, \quad P_{szz}(0,0,\varepsilon^*) = Q_{ssz}(0,0,\varepsilon^*) = Q_{zzz}(0,0,\varepsilon^*) = 0, \\ &P_{sz}(0,0,\varepsilon^*) = p_2, \quad P_{ss}(0,0,\varepsilon^*) = 2p_1, \quad P_{zz}(0,0,\varepsilon^*) = Q_{sz}(0,0,\varepsilon^*) = 0, \\ &Q_{ss}(0,0,\varepsilon^*) = -\frac{\varepsilon^*\beta}{(\alpha + u^*)^3}, \quad Q_{zz}(0,0,\varepsilon^*) = 0. \end{aligned}$$

Clearly,

$$\operatorname{sgn}\left[\frac{\partial(\mathrm{Re}\varphi)}{\partial\varepsilon}\right]_{\varepsilon=\varepsilon^*} < 0.$$

Denote $\Upsilon = -\frac{S_1(\varepsilon^*)}{\varphi'(\varepsilon^*)}$. □

D Proof of Theorem 4.1

Proof The equilibria $E_1(0,0)$, $E_2(N, \frac{\beta}{k(\alpha+N)})$, and $E_-^*(u_-^*, m_-^*)$ of the temporal system (2.3) also satisfy spatial system (2.4). Define a two-dimensional domain $\Omega : \{\mathbf{x} = (x, y) | 0 < x < V, 0 < y < V\}$ and its boundary $\partial\Omega$ is a rectangle. As is known the following spatial eigenvalue problem

$$\begin{cases} \nabla^2\mathbf{G} + n^2\mathbf{G} = 0, & \mathbf{x} \in \Omega, \\ \dfrac{\partial\mathbf{G}}{\partial\lambda} = 0, & \mathbf{x} \in \partial\Omega, \end{cases}$$

has eigenfunctions

$$\mathbf{G}_{p.q} = \mathbf{F}_{p.q}\cos\frac{p\pi x}{V}\cos\frac{q\pi y}{V}, \quad n^2 = \pi^2\left(\frac{p^2}{V^2} + \frac{q^2}{V^2}\right),$$

where p and q are integers, $\mathbf{x} = (x, y)$, and $\mathbf{F}_{p,q}$ are Fourier coefficients. Linearizing system (2.4) at arbitrary steady state $E(u, m)$ yields

$$\begin{cases} \dfrac{\partial\mathbf{W}}{\partial t} = \Gamma\mathbf{W} := D_1\nabla^2\mathbf{W} + \bar{J}\mathbf{W}, & \mathbf{x} \in \Omega, \\ \dfrac{\partial\mathbf{W}}{\partial\upsilon} = 0, & \mathbf{x} \in \partial\Omega, \\ \mathbf{W}(\mathbf{x}, 0) = \mathbf{W}_0(\mathbf{x}), & \mathbf{x} \in \Omega, \end{cases} \tag{D.1}$$

where

$$\bar{J} = \begin{pmatrix} \bar{j}_{11} & \bar{j}_{12} \\ \bar{j}_{21} & \bar{j}_{22} \end{pmatrix}, \quad \mathbf{W} = \begin{pmatrix} \tilde{u} - u \\ \tilde{m} - m \end{pmatrix}, \quad D_1 = \begin{pmatrix} d_u & 0 \\ 0 & d_m \end{pmatrix},$$

with

$$\begin{aligned} \bar{j}_{11} &= \frac{1}{N^2}\Big[-3\eta_1u^2m + 3\delta\eta_3u^2 - 2N(\eta_2 - \eta_1)um + 2N\delta(d_0 - b_0 - \eta_3)u \\ &\quad + N^2\eta_2m + N^2\delta(b_0 - d_0)\Big], \\ \bar{j}_{12} &= \frac{u(N-u)}{N^2}(\eta_1u - N\eta_2), \quad \bar{j}_{21} = \frac{\alpha\beta\varepsilon}{(u+\alpha)^2}, \quad \bar{j}_{22}^* = -Nk\varepsilon. \end{aligned}$$

Now search for solutions $\mathbf{G}_{p,q}(\mathbf{x}, t)$ of (D.1) in the following form

$$\mathbf{G}_{p,q}(\mathbf{x}, t) = \sum_{p,q} \mathbf{F}_{p,q} e^{\lambda(n^2)t} \cos\frac{p\pi x}{V} \cos\frac{q\pi y}{V}. \tag{D.2}$$

Substituting (D.2) into (D.1) yields

$$\lambda^2 - \mathrm{Tr}(n^2)\lambda + \mathrm{Det}(n^2) = 0, \tag{D.3}$$

where

$$\begin{aligned} \mathrm{Tr}(n^2) &= -(d_u + d_m)n^2 + \bar{j}_{11} + \bar{j}_{22}, \\ \mathrm{Det}(n^2) &= d_u d_m n^4 - (\bar{j}_{11} d_m + \bar{j}_{22} d_u)n^2 + \bar{j}_{11}\bar{j}_{22} - \bar{j}_{12}\bar{j}_{21}. \end{aligned}$$

(I) When $E(u, m) = E_1(0, 0)$, Eq. (D.3) has two eigenvalues $\lambda_{1n} = -d_u n^2 + \delta(b_0 - d_0)$ and $\lambda_{2n} = -d_m n^2 - Nk\varepsilon$. We know that $\lambda_{2n} < 0$ always is valid. Thus, the stability of $E_1(0, 0)$ relies on λ_{1n}. If $d_0 > b_0$, then $\lambda_{1n} < 0$ holds for all n. However, there exists $n = 0$ such that $\lambda_{10} = b_0 - d_0 > 0$ when $d_0 < b_0$. Therefore, $E_1(0, 0)$ is spatially unstable when $d_0 < b_0$.
(II) When $E(u, m) = E_2(N, \frac{\beta}{k(\alpha+N)})$, $\lambda_{1n} = -d_m n^2 - Nk\varepsilon$ and $\lambda_{2n} = -d_u n^2 + \delta(c_0 - a_0) - \frac{\beta(\eta_1+\eta_2)}{k(N+\alpha)}$ are eigenvalues of (D.3). Clearly, $\lambda_{1n} < 0$ holds for all n. Further, $\lambda_{2n} < 0$ is true for all n when $\delta(c_0 - a_0) < \frac{\beta(\eta_1+\eta_2)}{k(N+\alpha)}$. Conversely, there exists $n = 0$ such that $\lambda_{2n} = \delta(c_0 - a_0) - \frac{\beta(\eta_1+\eta_2)}{k(N+\alpha)} > 0$ when $\delta(c_0 - a_0) > \frac{\beta(\eta_1+\eta_2)}{k(N+\alpha)}$.
(III) When $E(u, m) = E_-^*(u_-^*, m_-^*)$, we have $\bar{J}|_{E=E_-^*} = J^*$. It is clear that $j_{21}^* = \frac{\alpha\beta\varepsilon}{(u^*+\alpha)^2} > 0$ and $j_{22}^* = -Nk\varepsilon < 0$. Easily known $b_0 > b_0^{**}$ and $b_0 < \hat{b}_0$ enable $j_{11}^* < 0$ and $j_{12}^* < 0$ to hold, respectively. Therefore, if $b_0 > \max\{b_0^*, b_0^{**}\}$ or $b_0^{**} < b_0 < \hat{b}_0$, then $\mathrm{Tr}(n^2) < 0$ and $\mathrm{Det}(n^2) > 0$ are valid for all n, which implies that $E_-^*(u_-^*, m_-^*)$ is spatially stable. This completes the proof. □

E Proof of Theorem 4.2

Proof Following Theorem 3.1 (III), the positive equilibrium $E_-^*(u_-^*, m_-^*)$ for the non-diffusive system (2.3) is stable when $\varepsilon > \varepsilon^*$ and $b_0 > b_0^*$. Turing instability occurs when the spatially steady state $E_-^*(u_-^*, m_-^*)$ for the diffusive system (2.4) loses stability due to small amplitude heterogeneous perturbations around $E_-^*(u_-^*, m_-^*)$ in a two-dimensional square domain. Assuming $\varepsilon > \varepsilon^*$ and $b_0 > b_0^*$, $\mathrm{Tr}(n^2) < 0$ constantly holds, so Turing instability is only possible in the case of $\mathrm{Det}(n^2) < 0$. For convenience, define

$$\varpi(n^2) := \mathrm{Det}(n^2) = d_u d_m n^4 - \left(j_{11}^* d_m + j_{22}^* d_u\right) n^2 + j_{11}^* j_{22}^* - j_{12}^* j_{21}^*. \tag{E.1}$$

When $b_0 > b_0^*$, one knows that $\det(J^*) = j_{11}^* j_{22}^* - j_{12}^* j_{21}^* > 0$. From (E.1), $\varpi(n^2) < 0$ has the possibility to hold when

$$\chi(d_u, d_m) = j_{11}^* d_m + j_{22}^* d_u > 0.$$

Combining (E.1) with $\mathrm{tr}(J^*) = j_{11}^* + j_{22}^* < 0$, it is evident that $d_u \neq d_m$ and j_{11}^* and j_{22}^* have opposite signs. One can see $j_{11}^* > 0$ since $j_{22}^* < 0$. We obtain $j_{12}^* < 0$ since $j_{11}^* > 0$, $j_{21}^* > 0$, $j_{22}^* < 0$, and $\det(J^*) = j_{11}^* j_{22}^* - j_{12}^* j_{21}^* > 0$. The minimum value of $\varpi(n^2)$ at $n_{\min}^2$ is

$$\min_n \varpi(n^2) = j_{11}^* j_{22}^* - j_{12}^* j_{21}^* - \frac{(j_{11}^* d_m + j_{22} d_u)^2}{4 d_u d_m},$$

where

$$n_{\min}^2 = \frac{j_{11}^* d_m + j_{22}^* d_u}{2 d_u d_m}.$$

From $\min_n \varpi(n^2) = 0$, we obtain

$$j_{11}^* j_{22}^* - j_{12}^* j_{21}^* = \frac{(j_{11}^* d_m + j_{22}^* d_u)^2}{4 d_u d_m}.$$

Let

$$\begin{aligned}\Lambda(d_u, d_m) &:= (j_{11}^* d_m + j_{22} d_u)^2 - 4 d_u d_m (j_{11}^* j_{22}^* - j_{12}^* j_{21}^*) \\ &= j_{11}^{*2} d_m^2 + j_{22}^{*2} d_u^2 + 2 d_u d_m (2 j_{12}^* j_{21}^* - j_{11}^* j_{22}^*).\end{aligned}$$

Set $\phi = \frac{d_m}{d_u}$, then

$$\Lambda(d_u, d_m) = j_{11}^{*2} \phi^2 + 2(2 j_{12}^* j_{21}^* - j_{11}^* j_{22}^*)\phi + j_{22}^{*2} = 0.$$

According to $\chi(d_u, d_m) = 0$, we get

$$\phi = -\frac{j_{22}^*}{j_{11}^*} \triangleq \phi^*.$$

Since $j_{12}^* < 0$, $j_{21}^* > 0$ and $\det(J^*) > 0$, we have

$$4(2 j_{12}^* j_{21}^* - j_{11}^* j_{22}^*)^2 - 4 j_{11}^{*2} j_{22}^{*2} = 16 j_{21} j_{12} (j_{12}^* j_{21}^* - j_{11}^* j_{22}^*) > 0.$$

Thus the equation $\Lambda(d_u, d_m) = 0$ has two positive roots as follows

$$\phi_1 = \frac{j_{11}^* j_{22}^* - 2 j_{21}^* j_{12}^* + \sqrt{(2 j_{21}^* j_{12}^* - j_{11}^* j_{22}^*)^2 - j_{11}^{*2} j_{22}^{*2}}}{j_{11}^{*2}},$$

$$\phi_2 = \frac{j_{11}^* j_{22}^* - 2j_{21}^* j_{12}^* - \sqrt{(2j_{21}^* j_{12}^* - j_{11}^* j_{22}^*)^2 - j_{11}^{*2} j_{22}^{*2}}}{j_{11}^{*2}}.$$

Easily one can get

$$0 < \phi_2 < \phi^* < \phi_1.$$

If $\phi = \frac{d_m}{d_u} > \phi_1$, then $\min_n \varpi(n^2) < 0$ and $\chi(d_u, d_m) > 0$. Thus, $E_-^*(u_-^*, m_-^*)$ is spatially unstable which suggests that Turing instability emerges. Denote $d_m^c = \phi_1 d_u$, then the critical wavenumber is

$$n_c^2 = \frac{j_{11}^* d_m^c + j_{22}^* d_u}{2 d_u d_m^c}.$$

□

F Proof of Theorem 4.3

Proof When $\mathrm{Tr}(n^2) = 0$ and $\mathrm{Det}(n^2) > 0$, (D.3) has pure imaginary roots. Take ε as the bifurcation parameter and denote

$$\varepsilon^{**} = -\frac{(d_u + d_m)n^2}{Nk} + \varepsilon^*.$$

If $\varepsilon = \varepsilon^{**}$, then $\mathrm{Tr}(n^2) = 0$. Letting $\varepsilon = \varepsilon^{**}$, it is clear that $\varepsilon^{**} > \frac{j_{11}^* d_m}{N k d_u}$ allows $[j_{11}^* d_m + j_{22}^* d_u]|_{\varepsilon=\varepsilon^{**}} < 0$. It is known that $b_0 > b_0^*$ leads to $\det(J^*)|_{\varepsilon=\varepsilon^{**}} = j_{11}^* j_{22}^* - j_{21}^* j_{12}^* > 0$. Therefore, $\mathrm{Det}(n^2)|_{\varepsilon=\varepsilon^{**}} > 0$ when $\varepsilon^{**} > \frac{j_{11}^* d_m}{N k d_u}$ and $b_0 > b_0^*$.

From (D.3), we obtain

$$\mathrm{Re}\left(\frac{d\lambda}{d\varepsilon}\right)_{\varepsilon=\varepsilon^{**}} = -\frac{Nk}{2} \neq 0.$$

The transversality condition is valid, so the Hopf bifurcation occurs at $\varepsilon = \varepsilon^{**}$. □

G Proof of Theorem 4.4

Proof Let $\mathrm{Det}(n^2) = 0$, that is

$$d_u d_m n^4 - (j_{11}^* d_m - Nk\varepsilon d_u)n^2 - j_{11}^* Nk\varepsilon - \frac{j_{12}^* \alpha\beta\varepsilon}{(u+\alpha)^2} = 0. \tag{G.1}$$

Denote $\hat{d}_u = \frac{j_{11}^*(d_m + Nk\varepsilon)}{d_m + Nk\varepsilon}$. Clearly, the Turing bifurcation curve cannot interact with the Hopf bifurcation curve $\varepsilon = \varepsilon^{**}$ when $d_u > \hat{d}_u$ and $\eta_2 < \frac{\eta_1 u_-^*}{N}$. If $d_u < \hat{d}_u$ and

$\eta_2 < \frac{\eta_1 u_-^*}{N}$, then substituting $\varepsilon = \varepsilon^{**}$ into (G.1) yields

$$\beta(n) = \frac{\left(Nkj_{11}^*\varepsilon^{**} + (j_{11}^* d_m - Nkd_u\varepsilon^{**})n^2 - d_u d_m n^4\right)(u_-^* + \alpha)^2}{(-j_{11}^*\alpha\varepsilon^{**})}, \quad n \in [1, n^*], \tag{G.2}$$

where

$$n^* = \left[\frac{Nkd_u\varepsilon^{**} - j_{11}^* d_m + \sqrt{(Nkd_u\varepsilon^{**} - j_{11}^* d_m)^2 + 4d_u d_m Nkj_{11}^*\varepsilon^{**}}}{-2d_u d_m}\right],$$

and $[\cdot]$ represents the integer part function. Let

$$f(z) = Nkj_{11}^*\varepsilon^{**} + (j_{11}^* d_m - Nkd_u\varepsilon^{**})z - d_u d_m z^2,\ z \in [1, n^{*2}].$$

One can see that $f'(z) \geq 0$ for $z \leq z^*$ and $f'(z) < 0$ for $z > z^*$, where

$$z^* = \frac{j_{11}^* d_m - Nkd_u\varepsilon^{**}}{2d_u d_m}.$$

Let

$$n_* = \begin{cases} 1, & \text{if } z^* \leq 1, \\ [\sqrt{z^*}], & \text{if } \beta([\sqrt{z^*}]+1) \leq \beta([\sqrt{z^*}]), \quad 1 < \sqrt{z^*} < n^*, \\ [\sqrt{z^*}]+1, & \text{if } \beta([\sqrt{z^*}]) \leq \beta([\sqrt{z^*}]+1), \quad 1 < \sqrt{z^*} < n^*. \end{cases}$$

There exists $n_* \in [1, n^*]$ such that $\beta^* = \beta(n_*) = \max\limits_{1\leq n\leq n^*} \beta(n)$. Therefore, system (2.4) undergoes Turing–Hopf bifurcation at point

$$(\beta^*, \varepsilon^{**}) = \left(\frac{\left(Nkj_{11}^*\varepsilon^{**} + (j_{11}^* d_m - Nkd_u\varepsilon^{**})n_*^2 - d_u d_m n_*^4\right)(u_-^* + \alpha)^2}{(-j_{11}^*\alpha\varepsilon^{**})}, \varepsilon^{**}\right).$$

□

Acknowledgements The research of Haihui Cheng was partially supported by the National Natural Science Foundation of China (No.12271308) and the China Scholarship Council. The research of Hao Wang was partially supported by the Natural Sciences and Engineering Research Council of Canada (Individual Discovery Grant RGPIN-2020-03911 and Discovery Accelerator Supplement Award RGPAS-2020-00090) and the Canada Research Chairs program (Tier 1 Canada Research Chair Award). The research of Xinzhu Meng was partially supported by the National Natural Science Foundation of China (No.12271308).

Data availability Data sharing is not applicable to this article as no datasets were generated or analyzed during the current study.

Declarations

Conflict of interest All authors certify that they have no affiliations with or involvement in any organization or entity with any financial interest or non-financial interest in the subject matter or materials discussed in this manuscript.

References

Aydogmus O (2018) Discovering the effect of nonlocal payoff calculation on the stabilty of ess: Spatial patterns of hawk–dove game in metapopulations. J Theor Biol 442:87–97. https://doi.org/10.1016/j.jtbi.2018.01.016

Behar H, Brenner N, Louzoun Y (2014) Coexistence of productive and non-productive populations by fluctuation-driven spatio-temporal patterns. Theor Popul Biol 96:20–9. https://doi.org/10.1016/j.tpb.2014.06.002

Berres S, Ruiz-Baier R (2011) A fully adaptive numerical approximation for a two-dimensional epidemic model with nonlinear cross-diffusion. Nonlinear Anal-Real World Appl 12(5):2888–2903. https://doi.org/10.1016/j.nonrwa.2011.04.014

Bonnefon JF, Shariff A, Rahwan I (2016) The social dilemma of autonomous vehicles. Science 352(6293):1573–6. https://doi.org/10.1126/science.aaf2654

Charness G, Cobo-Reyes R, Jiménez N (2014) Identities, selection, and contributions in a public-goods game. Games Econ Behav 87:322–338. https://doi.org/10.1016/j.geb.2014.05.002

Cheng HH, Meng XZ, Hayat T, Hobiny A (2022) Dynamics analysis for a prey-predator evolutionary game system with delays. Dyn Games Appl 1–28. https://doi.org/10.1007/s13235-022-00464-w

Cheng H, Meng X (2023) Evolution of cooperation in multigame with environmental space and delay. Biosystems 223:104801. https://doi.org/10.1016/j.biosystems.2022.104801

Cheng HH, Meng XZ, Hayat T, Hobiny A (2023) Multistability and bifurcation analysis for a three-strategy game system with public goods feedback and discrete delays. Chaos Solit Fractals 175:114011. https://doi.org/10.1016/j.chaos.2023.114011

Chowdhury SN, Kundu S, Perc M, Ghosh D (2021) Complex evolutionary dynamics due to punishment and free space in ecological multigames. Proc R Soc A-Math Phys Eng Sci 477(2252):20210397. https://doi.org/10.1098/rspa.2021.0397

Chowdhury PR, Petrovskii S, Banerjee M (2021) Oscillations and pattern formation in a slow–fast prey–predator system. Bull Math Biol 83(11):110. https://doi.org/10.1007/s11538-021-00941-0

Conlin PL, Chandler JR, Kerr B (2014) Games of life and death: antibiotic resistance and production through the lens of evolutionary game theory. Curr Opin Microbiol 21:35–44. https://doi.org/10.1016/j.mib.2014.09.004

Cressman R, Vickers GT (1997) Spatial and density effects in evolutionary game theory. J Theor Biol 184(4):359–69. https://doi.org/10.1006/jtbi.1996.0251

Deegan RD (2000) Pattern formation in drying drops. Phys Rev E 61(1):475–85. https://doi.org/10.1103/physreve.61.475

Diggle SP, Griffin AS, Campbell GS, West SA (2007) Cooperation and conflict in quorum-sensing bacterial populations. Nature 450(7168):411–4. https://doi.org/10.1038/nature06279

Duong MH, Han TA (2016) Analysis of the expected density of internal equilibria in random evolutionary multi-player multi-strategy games. J Math Biol 73(6–7):1727–1760. https://doi.org/10.1007/s00285-016-1010-8

Duong MH, Han TA (2016) On the expected number of equilibria in a multi-player multi-strategy evolutionary game. Dyn Games Appl 6(3):324–346. https://doi.org/10.1007/s13235-015-0148-0

Fallucchi F, Luccasen RA, Turocy TL (2019) Identifying discrete behavioural types: a re-analysis of public goods game contributions by hierarchical clustering. J Econ Sci Assoc 5(2):238–254. https://doi.org/10.1007/s40881-018-0060-7

Figueiredo ART, Wagner A, Kummerli R (2021) Ecology drives the evolution of diverse social strategies in *Pseudomonas aeruginosa*. Mol Ecol 30(20):5214–5228. https://doi.org/10.1111/mec.16119

Griffin AS, West SA, Buckling A (2004) Cooperation and competition in pathogenic bacteria. Nature 430(7003):1024–7. https://doi.org/10.1038/nature02744

Hauert C (2002) Effects of space in 2 × 2 games. Int J Bifurc Chaos 12(07):1531–1548. https://doi.org/10.1142/S0218127402005273

Hauert C, Saade C, McAvoy A (2019) Asymmetric evolutionary games with environmental feedback. J Theor Biol 462:347–360. https://doi.org/10.1016/j.jtbi.2018.11.019
Heggerud CM, Wang H, Lewis MA (2020) Transient dynamics of a stoichiometric cyanobacteria model via multiple-scale analysis. SIAM J Appl Math 80(3):1223–1246. https://doi.org/10.1137/19m1251217
Heggerud CM, Wang H, Lewis MA (2022) Coupling the socio-economic and ecological dynamics of cyanobacteria: single lake and network dynamics. Ecol Econ 194:107324. https://doi.org/10.1016/j.ecolecon.2021.107324
Hofbauer J, Sigmund K (1998) Evolutionary games and population dynamics. Cambridge University Press. https://doi.org/10.1017/CBO9781139173179
Jia D, Zhang T, Yuan S (2019) Pattern dynamics of a diffusive toxin producing phytoplankton–zooplankton model with three-dimensional patch. Int J Bifurc Chaos 29(4):1930011. https://doi.org/10.1142/S0218127419300118
Julou T, Mora T, Guillon L, Croquette V, Schalk IJ, Bensimon D, Desprat N (2013) Cell-cell contacts confine public goods diffusion inside *Pseudomonas aeruginosa* clonal microcolonies. Proc Natl Acad Sci USA 110(31):12577–82. https://doi.org/10.1073/pnas.1301428110
Kerr B, Riley MA, Feldman MW, Bohannan BJ (2002) Local dispersal promotes biodiversity in a real-life game of rock–paper–scissors. Nature 418(6894):171–4. https://doi.org/10.1038/nature00823
Kirkup BC, Riley MA (2004) Antibiotic-mediated antagonism leads to a bacterial game of rock–paper–scissors in vivo. Nature 428(6981):412–4. https://doi.org/10.1038/nature02429
Kummerli R, Colliard C, Fiechter N, Petitpierre B, Russier F, Keller L (2007) Human cooperation in social dilemmas: comparing the Snowdrift game with the Prisoner's dilemma. Proc R Soc B Biol Sci 274(1628):2965–70. https://doi.org/10.1098/rspb.2007.0793
Lambert G, Vyawahare S, Austin RH (2014) Bacteria and game theory: the rise and fall of cooperation in spatially heterogeneous environments. Interface Focus 4(4):20140029. https://doi.org/10.1098/rsfs.2014.0029
Lett C, Auger P, Gaillard JM (2004) Continuous cycling of grouped vs. solitary strategy frequencies in a predator–prey model. Theor Popul Biol 65(3):263–70. https://doi.org/10.1016/j.tpb.2003.10.005
Li J, Sun GQ, Jin Z (2014) Pattern formation of an epidemic model with time delay. Physica A 403:100–109. https://doi.org/10.1016/j.physa.2014.02.025
Li X, Jusup M, Wang Z, Li H, Shi L, Podobnik B, Stanley HE, Havlin S, Boccaletti S (2018) Punishment diminishes the benefits of network reciprocity in social dilemma experiments. Proc Natl Acad Sci USA 115(1):30–35. https://doi.org/10.1073/pnas.1707505115
Lotito G, Migheli M, Ortona G (2013) Is cooperation instinctive? Evidence from the response times in a public goods game. J Bioecon 15:123–133. https://doi.org/10.1007/s10818-012-9141-5
Lynn BK, De Leenheer P (2019) Division of labor in bacterial populations. Math Biosci 316:108257. https://doi.org/10.1016/j.mbs.2019.108257
MacLean RC, Gudelj I (2006) Resource competition and social conflict in experimental populations of yeast. Nature 441(7092):498–501. https://doi.org/10.1038/nature04624
Maini P, Painter K, Chau HP (1997) Spatial pattern formation in chemical and biological systems. J Chem Soc Faraday Trans 93(20):3601–3610. https://doi.org/10.1039/A702602A
Manna K, Volpert V, Banerjee M (2021) Pattern formation in a three-species cyclic competition model. Bull Math Biol 83(5):52. https://doi.org/10.1007/s11538-021-00886-4
Milinski M, Semmann D, Krambeck HJ (2002) Reputation helps solve the 'tragedy of the commons'. Nature 415(6870):424–6. https://doi.org/10.1038/415424a
Milne R, Bauch CT, Anand M (2022) Local overfishing patterns have regional effects on health of coral, and economic transitions can promote its recovery. Bull Math Biol 84(4):46. https://doi.org/10.1007/s11538-022-01000-y
Mridha S, Kummerli R (2022) Enforced specialization fosters mutual cheating and not division of labour in the bacterium *Pseudomonas aeruginosa*. J Evol Biol 35(5):719–730. https://doi.org/10.1111/jeb.14001
Nowak MA (2006) Evolutionary dynamics: exploring the equations of life. Harvard University Press. https://doi.org/10.2307/j.ctvjghw98
Pal S, Banerjee M, Ghorai S (2020) Effects of boundary conditions on pattern formation in a nonlocal prey–predator model. Appl Math Model 79:809–823. https://doi.org/10.1016/j.apm.2019.10.061
Pal S, Petrovskii S, Ghorai S, Banerjee M (2021) Spatiotemporal pattern formation in 2d prey–predator system with nonlocal intraspecific competition. Commun Nonlinear Sci Numer Simul 93:105478. https://doi.org/10.1016/j.cnsns.2020.105478

Rand DG, Tomlin D, Bear A, Ludvig EA, Cohen JD (2017) Cyclical population dynamics of automatic versus controlled processing: an evolutionary pendulum. Psychol Rev 124(5):626–642. https://doi.org/10.1037/rev0000079

Rankin DJ, Bargum K, Kokko H (2007) The tragedy of the commons in evolutionary biology. Trends Ecol Evol 22(12):643–51. https://doi.org/10.1016/j.tree.2007.07.009

Ratzke C, Gore J (2016) Self-organized patchiness facilitates survival in a cooperatively growing *Bacillus subtilis* population. Nat Microbiol 1(5):16022. https://doi.org/10.1038/nmicrobiol.2016.22

Riehl C, Frederickson ME (2016) Cheating and punishment in cooperative animal societies. Philos Trans R Soc B Biol Sci 371(1687):20150090. https://doi.org/10.1098/rstb.2015.0090

Schuster S, Kreft JU, Brenner N, Wessely F, Theissen G, Ruppin E, Schroeter A (2010) Cooperation and cheating in microbial exoenzyme production-theoretical analysis for biotechnological applications. Biotechnol J 5(7):751–8. https://doi.org/10.1002/biot.200900303

Smith P, Schuster M (2019) Public goods and cheating in microbes. Curr Biol 29(11):R442–R447. https://doi.org/10.1016/j.cub.2019.03.001

Song Y, Peng Y, Zhang T (2021) The spatially inhomogeneous Hopf bifurcation induced by memory delay in a memory-based diffusion system. J Differ Equ 300:597–624. https://doi.org/10.1016/j.jde.2021.08.010

Song Y, Peng Y, Zhang T (2022) Double Hopf bifurcation analysis in the memory-based diffusion system. J Dyn Differ Equ 1–46. https://doi.org/10.1007/s10884-022-10180-z

Sun TA, Hilker FM (2021) Comparison between best-response dynamics and replicator dynamics in a social-ecological model of lake eutrophication. J Theor Biol 509:110491. https://doi.org/10.1016/j.jtbi.2020.110491

Sun GQ, Jin Z, Liu QX, Li LI (2009) Spatial pattern in an epidemic system with cross-diffusion of the susceptible. J Biol Syst 17(01):141–152. https://doi.org/10.1142/S0218339009002843

Tilman AR, Plotkin JB, Akcay E (2020) Evolutionary games with environmental feedbacks. Nat Commun 11(1):915. https://doi.org/10.1038/s41467-020-14531-6

Wakano JY, Nowak MA, Hauert C (2009) Spatial dynamics of ecological public goods. Proc Natl Acad Sci USA 106(19):7910–4. https://doi.org/10.1073/pnas.0812644106

Walgraef D (2012) Spatio-temporal pattern formation: with examples from physics, chemistry, and materials science. Springer Science & Business Media. https://doi.org/10.1007/978-1-4612-1850-0

Wang YH, Cheng DZ (2016) Dynamics and stability for a class of evolutionary games with time delays in strategies. Sci China Inf Sci 59(9):92209. https://doi.org/10.1007/s11432-016-5532-x

Wang M, Schaefer AL, Dandekar AA, Greenberg EP (2015) Quorum sensing and policing of *Pseudomonas aeruginosa* social cheaters. Proc Natl Acad Sci USA 112(7):2187–91. https://doi.org/10.1073/pnas.1500704112

Weitz JS, Eksin C, Paarporn K, Brown SP, Ratcliff WC (2016) An oscillating tragedy of the commons in replicator dynamics with game-environment feedback. Proc Natl Acad Sci USA 113(47):E7518–E7525. https://doi.org/10.1073/pnas.1604096113

Xu J, Shi J, Zhang H (2018) A leader-follower stochastic linear quadratic differential game with time delay. Sci China Inf Sci 61(11):112202. https://doi.org/10.1007/s11432-017-9293-4

Yamaguchi S, Iwasa Y (2021) Evolutionary game in an androdioecious population: coupling of outcrossing and male production. J Theor Biol 513:110594. https://doi.org/10.1016/j.jtbi.2021.110594

Yan S, Jia D, Zhang T, Yuan S (2020) Pattern dynamics in a diffusive predator–prey model with hunting co-operations. Chaos Solit Fractals 130:109428. https://doi.org/10.1016/j.chaos.2019.109428

Yuan H, Meng X (2022) Replicator dynamics of division of labor games with delayed payoffs in infinite populations. Chaos Solit Fractals 158:112058. https://doi.org/10.1016/j.chaos.2022.112058

Zhao S, Yuan S, Wang H (2022) Adaptive dynamics of a stoichiometric phosphorus–algae–zooplankton model with environmental fluctuations. J Nonlinear Sci 32(3):36. https://doi.org/10.1007/s00332-022-09794-w